Bulletin of Mathematical Biology (2025) 87:40
https://doi.org/10.1007/s11538-025-01417-1

Society for Mathematical Biology

ORIGINAL ARTICLE

Mathematical Model of CAR T-Cell Therapy for a B-Cell Lymphoma Lymph Node

Soukaina Sabir[1] · **Odelaisy León-Triana**[1,2] · **Sergio Serrano**[3] · **Roberto Barrio**[3] · **Victor M. Pérez-García**[1]

Received: 31 July 2024 / Accepted: 16 January 2025 / Published online: 7 February 2025

Abstract
CAR T-cell therapies have demonstrated significant success in treating B-cell leukemia in children and young adults. However, their effectiveness in treating B-cell lymphomas has been limited in comparison to leukemia. In this paper we present a mathematical model that elucidates the dynamics of diffuse large B-cell lymphoma and CAR T-cells in a lymph node. The mathematical model aids in understanding the complex interplay between the cell populations involved and proposes ways to identify potential underlying dynamical causes of treatment failure. We also study the phenomenon of immunosuppression induced by tumor cells and theoretically demonstrate its impact on cell dynamics. Through the examination of various response scenarios, we underscore the significance of product characteristics in treatment outcomes.

Keywords Mathematical modeling · Cancer dynamics · Immunotherapy · Tumor–immune system interactions · Mathematical oncology

1 Introduction

Non-Hodgkin's lymphoma (NHL) encompasses a diverse group of malignancies characterized by abnormal clonal proliferation of faulty immune system cells, either T-cells, B-cells, or both accounting for 3% of cancer diagnoses globally (Thandra et al. 2021). In adults, the majority of NHL cases are of type B (Sehn and Salles 2021). The most prevalent subtype among NHLs is the diffuse large B-cell lymphoma

✉ Soukaina Sabir
Soukaina.Sabir@uclm.es

1 Department of Mathematics, Mathematical Oncology Laboratory (MOLAB), Universidad de Castilla-La Mancha, Ciudad Real, Spain

2 Translational Research in Pediatric Oncology, Hematopoietic Transplantation and Cell Therapy, Hospital La Paz Institute for Health Research-IdiPAZ, Madrid, Spain

3 Department of Applied Mathematics, Computational Dynamics Group (CoDy), Universidad de Zaragoza, Zaragoza, Spain

(DLBCL), with an incidence as high as 7.2 per 100,000 individuals per year (Wang 2023).

Immunotherapies have emerged as a highly effective treatment option for hematological malignancies, with Chimeric Antigen Receptor (CAR) T-cell therapy being the most successful in use today. In these innovative therapies, first approved by the FDA only in 2017, T-cells are extracted from the patient's blood and undergo genetic engineering within a laboratory to introduce a chimeric antigen receptor (CAR) tailored to cancer cells. Subsequently, these modified T-cells are cultured and expanded, generating a robust population. Once infused back into the patient, the CAR T-cells recognize and bind to cancer cells by targeting specific proteins on their surface. This binding activates the CAR T-cells, initiating a robust immune response characterized by the release of cytotoxic substances, ultimately leading to the destruction of cancer cells (Stein et al. 2019; Sterner and Sterner 2021). This personalized immunotherapy has demonstrated remarkable success for adults with DLBCL (Sheikh et al. 2022) as well as other haematological malignancies (Zhang et al. 2022), and even non-cancerous diseases (Baker et al. 2023). Promising results have been observed with high response rates and even complete responses sustained for long periods of time in DLBCL (Cappell and Kochenderfer 2023). CAR T-cells are currently offering a glimmer of hope for treating refractory or relapsed haematological cancers. However, several uncertainties remain, including identifying which patients will respond to treatment, how to sustain the treatment's effectiveness, and the long-term tolerance of CAR T-cells (Zhang et al. 2022).

Unlike other treatments with simple pharmacokinetics, CAR T-cells have a complex dynamics once infused. They first expand upon encountering their target antigen, in the case of haematological cancers most often CD19. This antigen is expressed both in cancer and healthy B-cells. After a fast initial expansion phase, the removal of the target cells leads to a decrease in the CAR T population, also due to the exhaustion of T-cells. Thus, the use of mathematical models can be of value in comprehending the intricacies of CAR T-cell treatment and its effects. Indeed, many studies have employed diverse mathematical models to investigate various aspects of CAR T-cell therapies on different cancers (Sahoo et al. 2020; Pérez-García et al. 2021; Barros et al. 2021; Bodnar et al. 2023; Li et al. 2023; Brummer et al. 2022; Mahasa et al. 2022; Barros et al. 2021; Owens and Bozic 2021; Liu et al. 2022; León-Triana et al. 2021b; Martínez-Rubio et al. 2021; León-Triana et al. 2021a; Kimmel et al. 2021).

Interestingly, despite the high incidence of lymphoma being the cancer type with more patients treated by CAR T-cells by far, the number of mathematical models addressing its treatments has been very small. Before the CAR T era, Roesch et al. (2013) adapted Kuznetsov's model, originally developed to describe leukemia in mice, to describe the interaction between a proliferating Non-Hodgkin's Lymphoma, an anti-tumor immune response, and the impact of chemotherapy on both the tumor and immune system. Notably, certain research findings indicate that more intensive therapies may lead to suboptimal tumor control. The objective of their work was to provide a plausible explanation for some of the paradoxical effects observed after chemotherapy therapy in lymphomas, while considering the significant anti-tumor role played by the immune system.

In a recent study, Kimmel et al. (2021) studied the dynamics and relationships between normal T-cells, CAR T-cells, and tumor cells in diffuse large B-cell lymphoma (DLBCL). The significance of this model lies in its depiction of cure as a stochastic event, highlighting the unpredictable nature of tumor eradication. This model can be applied to evaluate the effectiveness of CAR T-cell therapy in DLBCL and gain further insight into the impact of deterministic and stochastic factors on the outcomes. However, that model did not incorporate two relevant biological elements: the immunosuppression of T-cell action by both tumor cells and their microenvironment and the stimulation of CAR T-cell proliferation by the tumor antigens. These elements can profoundly impact in the treatment response and population dynamics in cases of diffuse large B-Cell lymphoma. Immunosuppression shapes the immune response and influences treatment outcomes, as highlighted by previous research (León-Triana et al. 2021a; Kuznetsov et al. 1994). Incorporating immunosuppression into the model is essential for a more realistic representation of the intricate interplay between the immune system and the lymphoma microenvironment, specially taking into account the compact nature of these tumors. Additionally, CAR T-cell proliferation after encountering tumor cells is a significant contributor to the efficacy of CAR T-cell therapy, as indicated by previous studies (León-Triana et al. 2021b; Martínez-Rubio et al. 2021; Barros et al. 2021), and it is certainly the leading contribution to expansion during the initial stages of response to treatment. Integrating all of these aspects into the modelling approach would enhance our ability to simulate and predict CAR T-cell behavior, providing a more nuanced mechanistic understanding of the lymphoma response to these therapies.

In this study, our goal is to address current knowledge gaps by crafting a simple mathematical model. This model aims to clarify the dynamic interplay between CAR T-cells and Lymphoma B-cells, specifically within the intricate microenvironment of lymph nodes-also termed lymph node area. Lymph nodes, small bean-shaped structures integral to the lymphatic system, constitute a network of vessels and organs crucial for immune function. Distributed throughout the body and concentrated in specific regions like the neck, armpits, groin, chest, and abdomen, these regions collectively constitute what is commonly referred to as lymph node areas. The focus on this anatomical context enhances our ability to capture the nuanced complexities of the cellular dynamics characterizing the interaction between CAR T-cells and lymphoma B-cells within a lymph node area. We provide a comprehensive explanation of the assumptions, requirements, and equations utilized in our model. Furthermore, we derive the mathematical properties of the model and thoroughly discuss the plausibility of our proposed parameters.

2 Mathematical Model

2.1 Model Development

In this study, we build a mechanistic model able to describe mechanistically the response to CAR-T treatments of non-Hodgkin's B-cell lymphoma in a lymph node area. Our mathematical model accounts for the time-evolution of two cellular pop-

ulations. Let us denote the number of CAR T-cells and lymphoma B-cells as $C(t)$ and $L(t)$ respectively, where t stands for time. The system of differential equations governing the dynamics of these populations will be taken to be:

$$\frac{dC}{dt} = \sigma(t) + \beta \frac{CL}{H+L} - \gamma \frac{CL}{G+C} - \frac{C}{\tau_C}, \tag{1a}$$

$$\frac{dL}{dt} = \rho L - \alpha LC. \tag{1b}$$

The first term in Eq. (1a) accounts for a external contribution to the CAR-T compartment given by the (in general) time dependent function $\sigma(t)$, that in our study will be assumed to be constant. This term models the influx of CAR T-cells arriving from other body sites into the lymph node area under investigation, reflecting a background level of CAR T-cell inflow from systemic circulation. In general, during the expansion phase, the contribution of this term will be negligible since most of the dynamics will be driven by local activation due to CAR T-cell interaction with the tumor antigen. However, when the antigen is depleted locally, the contribution of normal B-cell generation in the bone marrow will lead to some activation of the remaining CAR T-cells and will lead to a small constant flux through the body, that is accounted for in this term (Serrano et al. 2024).

The second term in Eq. (1a) accounts for the stimulation of CAR T-cell proliferation after their encounters with lymphoma cells. This term describes the rate at which CAR T-cells expand in the region of B-cell lymphoma due to the presence of tumor cells and is expected to be the main local contribution to the treatment expansion. It is important to point out that the rate of stimulation reaches a maximum value when the number of lymphoma cells is large. The parameter β measures the maximum mitotic stimulation after encounters with lymphoma cells, and H measures the lymphoma cell population that provides half of the maximum stimulation, i.e. when $L = H$, stimulation is $\beta/2$. This type of terms have been used previously (León-Triana et al. 2021a), and are preferable to other similar stimulation terms without any saturation used in the literature (Adhikarla et al. 2021; León-Triana et al. 2021b; Pérez-García et al. 2021). Unlike product terms of the form CL, they provide a limitation on the maximum expansion rate that the product can have, what reflects the maximum rate at which CAR T-cells can perform mitosis. In this study we will not include an independent term accounting for the proliferation stimulation related to the release of cytokines during CAR T-cell stimulation. Those cytokines have an accumulative effect due to their finite residence time in the lymph node area and could be described in different ways, either through a nonlocal activation term in Eq. (1a) or as an additional equation accounting the cytokine levels. Our choice here implicitly assumes that the residence time of cytokines is short so that the additional independent stimulation effect can be incorporated in the coefficient together with the direct stimulation β.

In tumors featuring a solid component, as it happens in lymph nodes, another key phenomenon is the induction of immune suppression by the tumor. This is delineated by the third term in Eq. (1a), signifying the deactivation of CAR T-cells by cancer cells. The maximum deactivation rate per cancer cell is denoted as γ, with the typical level of cellular saturation hovering around G. This type of terms have been employed

previously in the context of CAR T-cell therapy against brain tumors (León-Triana et al. 2021a). Here we assume that all of the tumor cells exert an immunosupressive effect on CAR T-cells, in line with the assumption of well-mixed populations implicit in the compartmental approach. In compact solid tumors one could consider alternatively terms with powers of the tumour cell number, e.g. $T^{2/3}$, to account for the fact that only the most accessible tumor population will be able to suppress CAR T-cell activity. However, probably only spatial models can account for the complexity of the space-time dynamics of the whole tumor-immune cell interaction.

The last term in Eq. (1a) describes the natural death (or inactivation) of activated CAR T-cells, with a characteristic time τ_c, depending typically on the CAR-T product properties and the persistence time of the activation of T-cells.

Equation (1b) describes the dynamics of lymphoma cells. For simplicity we assume in the first term that the growth of the tumor cell population follows an exponential pattern with a growth rate $\rho > 0$. While some studies have applied a logistic growth model to lymphoma cells (Ganesh et al. 2023; Kuznetsov et al. 1994), we opted for a simpler approach by introducing an exponential growth term for the tumor (Roesch et al. 2013; Kimmel et al. 2021). This decision is informed by the observation that, in the early stages of tumor growth, both models demonstrate comparable dynamics for lymphoma cells and at the stage at which the disease is detected and treated the tumor has not typically hit any anatomical barriers. Untreated real malignant cancers in humans have probably a faster growth (Pérez-García et al. 2020), but after treatment the remnant tumor clonal composition is substantially reduced so that lower powers are expected to rule tumor growth (Ocaña-Tienda et al. 2023). The exponential growth term provides both a simple description of growth with a minimal number of parameters and a balance between evolutionary forces and geometrical constraints that are present in the natural history of cancers and more specifically in lymphomas at treatment stage.

The second term in Eq. (1b) assumes that CAR T-cells exert their anti-cancer effects through the law of mass action, where the killing rate is directly proportional to the product of the concentrations of CAR-T-cells and cancer cells (León-Triana et al. 2021a, b; Sahoo et al. 2020; Li et al. 2023). The parameter α is related to the probability of an encounter between CAR-T and $CD19^+$ cells per unit of time and cell leading to the elimination of the target cell. This term does not include a saturation factor since, unlike mitotic processes that require substantially longer times to complete, encounters of T-cells with tumor cells can lead to a fast release of the cytotoxic load and elimination of the target in minutes (Davenport et al. 2015). Here we will consider that most of the death is due to those single-hit events, although recent evidences suggest that other more complex scenarios are possible (Weigelin et al. 2021; Weigelin and Friedl 2022). Various investigations have employed similar terms to characterize anti-tumor effects of T-cells (León-Triana et al. 2021b; Martínez-Rubio et al. 2021; León-Triana et al. 2021a; Sahoo et al. 2020; Roesch et al. 2013; Li et al. 2023).

In addition, our model aims to reflect that CAR T-cells can become inactivated within the immunosuppressive tumor microenvironment. Indeed, large B-cell lymphoma originates from B lymphocytes, leading to the formation of solid masses or enlargements within the lymph nodes. The significant challenge in treating these cancers with CAR T-cells stems from the immunosuppressive tumor microenvironment (TME). This immunosuppression is orchestrated by various factors, including

pro-tumor cell populations, cytokine profiles, metabolic immunosuppression, and vasculature, among others (Cheever et al. 2022). The obstacle presented by the immunosuppressive tumor microenvironment (TME) is a critical factor contributing to the failure of CAR-T-cell therapies for these tumors. Consequently, we have prioritized immunosuppression as a focal point in our mathematical model, aiming to attain a comprehensive understanding of cell dynamics in the context of CAR T-cell therapy for large B-cell lymphomas (Sterner and Sterner 2021).

Previous studies on B-cell lymphoma have integrated the inactivation of immune cells upon exposure to tumor cells using mass-action terms (Kuznetsov et al. 1994; Owens and Bozic 2021; Roesch et al. 2013; Santurio et al. 2024). The addition of this saturating term for inactivation/exhaustion of CAR T-cells distinguishes this model from other CAR T-cell models (Viola and Lanzavecchia 1996; León-Triana et al. 2021a). The incorporation of these biological effects within the mathematical model enhances its ability to capture the nuanced dynamics of immune responses in B-cell lymphoma patients.

2.2 Parameter Estimation

The CAR-T inflow parameter σ, depends on the number of CAR T-cells present in the patient's body after treatment. An estimation of effector cell production for human diffuse large B-cell lymphoma from the work of Roesch et al. (2013) is approximately 2×10^5 cells per day. Assuming that the biological mechanisms governing effector cells are similar to those of CAR T-cells, we consider a plausible range for σ to be between 10^5 and 10^7 cells per day.

Next, the maximum mitotic rate denoted as β, which is linked to the stimulation effect of T-cells through interaction with the target, depends on the characteristics of the CAR-T product. We chose the range for this parameter to be between 0.1 and $0.9\,\text{day}^{-1}$, in accordance with values reported in previous works (León-Triana et al. 2021b; Stein et al. 2019), and aligning with the observation that stimulated CAR T-cells can undergo several mitotic divisions per day.

For current CAR-T products, the mean lifetime τ_C of activated CAR T-cells typically falls within the range of 1 to 4 weeks (Nayar et al. 2015; León-Triana et al. 2021b; Ghorashian et al. 2019). Lymphoma B-cells, being fast-growing malignant cancers, exhibit a proliferation rate ρ on the order of several weeks, albeit with considerable individual patient variation (Frølund et al. 2011; Lang et al. 1980; Tubiana 1989). Hence, we set ρ within the range of 0.01 to $0.2\,\text{day}^{-1}$.

An approximate range for the parameter H is between 10^7 and 10^{10} cells (Stein et al. 2019). This range indicates the lymphoma cell population at which significant stimulation from CAR T-cells is observed. In the context of effector cells and tumor inactivation, the rate was estimated in mice and human diffuse large B-cell lymphoma and equals $3.422 \times 10^{-10}\,\text{day}^{-1}\,\text{cell}^{-1}$, as indicated by Roesch et al. (2013) and Kuznetsov et al. (1994). For CAR T-cells, we choose the maximum rate of tumor inactivation γ within the range from 0 to $1\,\text{day}^{-1}$. The CAR-T concentration for half-maximal tumor inactivation, represented by G, takes values in the range of 10^6 to 10^9 cells. This parameter reflects the CAR-T cell density at which inactivation mech-

anisms, such as exhaustion or immunosuppression, achieve half of their maximum activity. We assume that the value of G is intrinsically linked to H, where G is a fraction of H, as inactivation mechanisms become prominent when stimulation begins to saturate. This relationship depends on factors like the CAR-T cells' sensitivity to overactivation, environmental constraints, and the therapy's specific dynamics. For an H range of 10^7 to 10^{10}, G can often be estimated proportionally, typically within the same order of magnitude but leaning toward the lower end. For instance, if stimulation saturates at $H = 10^7$, G is likely between 10^6 and 10^7, reflecting the early onset of inactivation processes, such as those seen in therapies where CAR-T cells are prone to exhaustion. Conversely, if H approaches 10^{10}, G may be higher, around 10^9, indicating a delayed onset of inactivation mechanisms.

Furthermore, CAR T-cells exhibit killing efficiency against tumor cells, with values ranging from 10^{-11} to 10^{-9} day^{-1} cell^{-1}, as documented in León-Triana et al. (2021b).

A comprehensive summary of the model parameters and their respective numerical values is presented in Table 1.

3 Equilibrium Points and Stability

3.1 Dimensionless Model

To study the equilibria and their stability in this section we will use a dimensionless form of Eqs. (1), redefining the cell populations and time as follows

$$\bar{C} = \frac{\rho}{\sigma} C, \quad \bar{L} = \frac{L}{H}, \quad \bar{t} = \rho t. \tag{2}$$

The dimensionless parameters are related to the dimensional ones in the following way

$$m_1 = \frac{\beta}{\rho}, \quad m_2 = \frac{\gamma H}{\rho G}, \quad m_3 = \frac{\sigma}{\rho G}, \quad m_4 = \frac{1}{\rho \tau_C}, \quad m_5 = \frac{\alpha \sigma}{\rho^2}. \tag{3}$$

Then, our dimensionless system becomes

$$\frac{d\bar{C}}{d\bar{t}} = 1 + m_1 \frac{\bar{C}\bar{L}}{1+\bar{L}} - m_2 \frac{\bar{C}\bar{L}}{1+m_3\bar{C}} - m_4 \bar{C}, \tag{4a}$$

$$\frac{d\bar{L}}{d\bar{t}} = \bar{L} - m_5 \bar{C}\bar{L}. \tag{4b}$$

To ensure the biological significance of this model, it is essential for the trajectories of the dynamical system described by Eq. (4) to be positively invariant. However, that follows easily from the facts that the axis $\bar{L} = 0$ is invariant and that within the first quadrant, it is evident that $d\bar{C}(t)/dt > 0$ when $\bar{C}(t) \ll 1$. Thus, the following proposition holds:

Table 1 Parameter values for Eqs. (1) used in this work: names, description, values, units and sources

Parameter	Description	Value	Units	Source
σ	External inflow of CAR T-cells	10^5–10^7	cells$\times$ day^{-1}	Roesch et al. (2013)
β	Mitotic stimulation of CAR T-cell proliferation by tumor cells	0.1–0.9	day^{-1}	Stein et al. (2019) León-Triana et al. (2021b)
H	Saturation to CAR-T cell stimulation rate	10^7–10^{10}	cells	Stein et al. (2019)
γ	Tumor inactivation rate	0–1	day^{-1}	Kuznetsov et al. (1994)
G	CAR-T inactivation rate saturation constant	10^6–10^9	cells	Estimated
τ_C	Activated CAR-T cell lifetime	7–14	days	León-Triana et al. (2021b)
ρ	Tumor growth rate	0.01–0.2	day^{-1}	León-Triana et al. (2021b)
α	Killing efficiency of CAR T-cells	10^{-11}–10^{-9}	$\text{day}^{-1} \times$ cells^{-1}	León-Triana et al. (2021b)

Proposition 1 *For any non-negative initial data given by* $(\overline{C_0}, \overline{L_0})$*, the trajectories of Eqs. (4) are positively invariant.*

The existence and uniqueness of trajectories are direct consequences of the C^∞ nature of the second term of the differential system within the first quadrant.

3.2 Steady States and Stability Analysis

Although Eqs. (4) are a pair of autonomous ODEs determining a planar dynamical system with a simple form, its phase space has a complex structure. To understand the different dynamics that are possible in this system we will first study the nullclines and equilibrium points focusing in the regions of biological significance. Equilibrium points of biological significance are those where both $\overline{C}$ and $\overline{L}$ are non-negative. It is important to note that all of the model parameters must be non-negative to represent the intended biological phenomena.

Equilibrium points for Eqs. (4) are found at the intersections of nullclines, where the curves along which $\dot{\overline{C}} = 0$ and $\dot{\overline{L}} = 0$ intersect. The first equilibrium point, denoted as

$$E_1 = \left(\frac{1}{m_4}, 0\right), \tag{5a}$$

is determined by examining the intersection of $\dot{\overline{C}} = 0$ and $\overline{L} = 0$. This point consistently exists and is characterized as positive. Its stability, however, hinges on the specific values of the system parameters.

Proposition 2 *The tumor-free equilibrium point* E_1 *is asymptotically stable if* $m_5 > m_4$*, and unstable if* $m_5 < m_4$*.*

Proof The eigenvalues of Jacobian at the equilibrium point are $\lambda_1 = -m_4$ and $\lambda_2 = 1 - m_5/m_4$. Thus, E_1 is asymptotically stable if $m_4 < m_5$.

Proposition 2 implies that it is possible to change the state of the system from the tumor bearing state to the tumor-free point. We will later make use of this result.

In addition to E_1, for certain parameter sets, there are two additional equilibria,

$$E_2 = \left(\frac{1}{m_5}, \overline{L}_2\right), \tag{5b}$$

$$E_3 = \left(\frac{1}{m_5}, \overline{L}_3\right), \tag{5c}$$

corresponding to the high-tumor load and low-tumor load coexistence equilibria, respectively, both (5b) and (5c) represent states in which CAR T-cells coexists with the tumor. In Eqs. (5b) and (5c), $\overline{L}_2$ and $\overline{L}_3$ are the solutions of

$$a\overline{L}^2 + b\overline{L} + c = 0, \tag{6}$$

with

$$a = -\frac{m_2}{1+m_3/m_5}, \quad b = m_1 + m_5 - m_4 - \frac{m_2}{1+m_3/m_5}, \quad c = m_5 - m_4.$$

Therefore,

$$\bar{L}_2 = \frac{-b-\sqrt{\Delta}}{2a}, \tag{7a}$$

$$\bar{L}_3 = \frac{-b+\sqrt{\Delta}}{2a}, \tag{7b}$$

where $\Delta = b^2 - 4ac$.

Obviously, the existence of these two equilibria only occurs when $\Delta \geq 0$. Let us see when this is the case.

Proposition 3 *Equilibria E_2 and E_3 exist iff*

- $m_5 \geq m_4$ *or,*
- $m_5 < m_4$ *and*
  - $m_2 \leq (1+m_3/m_5)\left(\sqrt{m_1} - \sqrt{m_4 - m_5}\right)^2$ *or,*
  - $m_2 \geq (1+m_3/m_5)\left(\sqrt{m_1} + \sqrt{m_4 - m_5}\right)^2$.

Proof The discriminant is given by

$$\Delta = \left(m_1 + m_5 - m_4 - \frac{m_2}{1+m_3/m_5}\right)^2 + 4\frac{m_2}{1+m_3/m_5}(m_5 - m_4). \tag{8}$$

If $m_5 \geq m_4$, both summands are positive and therefore the discriminant Δ is positive.

Now we have to analyse the case when $m_5 < m_4$. Defining $k = \frac{m_2}{1+m_3/m_5}$ we get $\Delta = k^2 - 2k(m_1 + m_4 - m_5) + (m_1 - m_4 + m_5)^2$. So Δ is positive if and only if $k \leq k_1$ or $k \geq k_2$, where $k_1 = (m_1 + m_4 - m_5) - 2\sqrt{m_1(m_4 - m_5)}$ and $k_2 = (m_1+m_4-m_5)+2\sqrt{m_1(m_4 - m_5)}$ are the roots of the above polynomial. Substituting k for its value and solving for m_2, we obtain the conditions of the statement.

To ensure that E_2 and E_3 hold biological significance, it is pertinent to investigate their positivity. Since $m_5 > 0$, the positivity of E_2 and E_3 hinges on the values of $\bar{L}_2$ and $\bar{L}_3$, respectively. The following proposition outlines the conditions that must be met for that to happen.

Proposition 4 *Assuming that E_2 and E_3 exist (see previous proposition):*

1. $\bar{L}_2 \geq 0 \Leftrightarrow$
   - $m_5 \geq m_4$ *or,*
   - $m_2 \leq (1+m_3/m_5)(m_1 + m_5 - m_4)$.
2. $\bar{L}_3 \geq 0 \Leftrightarrow m_2 \leq (1+m_3/m_5)(m_1 + m_5 - m_4)$ *and* $m_5 \leq m_4$.

Proof From Eq. (7a), $\bar{L}_2 \geq 0$ when the numerator is negative given that $a \leq 0$. To analyze the sign of the numerator, $-b - \sqrt{\Delta}$, we distinguish two cases. The first one corresponds to the case when $b \geq 0$ then $-b - \sqrt{\Delta} \leq 0$ hence $\bar{L}_2$ is positive. Since $b = m_1 + m_5 - m_4 - \frac{m_2}{1+m_3/m_5}$, this case occurs if and only if

$$m_2 \leq (1 + m_3/m_5)(m_1 + m_5 - m_4).$$

In the second case, corresponding to $b < 0$,

$$\bar{L}_2 \geq 0 \Leftrightarrow -b - \sqrt{\Delta} \leq 0 \Leftrightarrow -b \leq \sqrt{\Delta} \Leftrightarrow b^2 \leq \Delta \Leftrightarrow -4ac \geq 0$$
$$\Leftrightarrow c \geq 0 \Leftrightarrow m_5 \geq m_4.$$

Now, let us focus on proving the second part of the proposition. To do so let us consider $\bar{L}_3$, given by Eq. (7b). $\bar{L}_3 \geq 0 \Leftrightarrow -b+\sqrt{\Delta}$ is negative. This condition cannot hold if $b \leq 0$. Therefore, b must be positive (i.e., $m_2 \leq (1+m_3/m_5)(m_1+m_5-m_4)$). Furthermore, b must be larger than $\sqrt{\Delta}$. This leads to the inequality:

$$\Delta \leq b^2 \Leftrightarrow -4ac \leq 0 \Leftrightarrow c \leq 0 \Leftrightarrow m_5 \leq m_4.$$

In agreement with our statement.

It is worth noting that if $m_5 = m_4$, we will have either $\bar{L}_2 = 0$ (iff $b \leq 0$) or $\bar{L}_3 = 0$ (iff $b \geq 0$). In such a scenario, the equilibrium point coincides with E_1, where the tumor cell population is reduced to zero while the CAR T-cells persist.

Once the conditions for the positivity of the equilibria E_2 and E_3 have been established it is necessary to study the stability, since that would give us an idea of how biologically feasible it is to take the system to that state. To do so, we will calculate the possible local bifurcations that can occur for equilibria, thus getting the boundaries of the regions with different behaviour around them.

3.3 Local Bifurcations

Through bifurcation analysis (Guckenheimer and Holmes 1983; Wiggins 2003), we will explore how changes in the system parameters lead to different outcomes, such as stable coexistence, eradication of lymphoma cells, or immune escape.

Theorem 5 *The equilibria of Eqs. (4) undergo a transcritical bifurcation at $m_4 = m_5$:*

- *When $m_2 > m_1(1 + m_3/m_5)$, E_1 and E_2 experience a transcritical bifurcation.*
- *When $m_2 < m_1(1 + m_3/m_5)$, E_1 and E_3 experience a transcritical bifurcation.*

Proof According to Proposition 2, the stability of the equilibrium E_1 changes when $m_4 = m_5$. On the other hand, E_1 and E_2 coincide when $m_4 = m_5$ and $m_2 \geq m_1(1 + m_3/m_5)$. Whereas E_1 and E_3 coincide when $m_4 = m_5$ and $m_2 \leq m_1(1 + m_3/m_5)$.

Finally, since the Jacobian matrix for E_i, with $i = 2, 3$, is

$$J\left(\frac{1}{m_5}, \bar{L}_i\right) = \begin{pmatrix} \dfrac{m_1\bar{L}_i}{1+\bar{L}_i} - \dfrac{m_2\bar{L}_i}{(1+\frac{m_3}{m_5})^2} - m_4 & \dfrac{m_1}{m_5(1+\bar{L}_i)^2} - \dfrac{m_2}{m_5(1+\frac{m_3}{m_5})} \\ -m_5\bar{L}_i & 0 \end{pmatrix}, \tag{9}$$

it is clear that its determinant changes sign when $\bar{L}_i$ changes sign (note that when $\bar{L}_i = 0$, $J_{1,2}$ changes sign only when $m_2 = m_1(1 + m_3/m_5)$). This happens in the cases described above.

Remark: In both cases the equilibria of Eqs. (4) go from E_1 stable and E_i saddle when $m_5 > m_4$ to E_1 saddle and E_i stable when $m_5 < m_4$, where i is 2 or 3, depending on the value of m_2.

As discussed above E_2 and E_3 exist only under certain parametric conditions (see Proposition 3). The boundary between the different regions of existence for E_2 and E_3 is determined by a fold bifurcation.

Theorem 6 *The equilibria E_2 and E_3 of the dynamical system (4) undergo a fold bifurcation when $m_5 \leq m_4$ and $m_2 = (1 + m_3/m_5)\left(\sqrt{m_1} \pm \sqrt{m_4 - m_5}\right)^2$.*

Proof As stated in the proof of Proposition 3, the value of Δ cancels out when $m_5 \leq m_4$ and $m_2 = (1 + m_3/m_5)\left(\sqrt{m_1} \pm \sqrt{m_4 - m_5}\right)^2$. In this situation, $E_2 = E_3$; in the outer region, E_2 and E_3 exist and are distinct; and in the inner region, E_2 and E_3 do not exist.

Remark: If we fix the values of m_1, m_3 and m_4, the condition $m_2 = (1 + m_3/m_5)\left(\sqrt{m_1} \pm \sqrt{m_4 - m_5}\right)^2$ (with $m_5 \leq m_4$) determines a curve with two branches. The branches $m_2 = (1 + m_3/m_5)\left(\sqrt{m_1} - \sqrt{m_4 - m_5}\right)^2$ and $m_2 = (1 + m_3/m_5)\left(\sqrt{m_1} + \sqrt{m_4 - m_5}\right)^2$ meet at the point $m_5 = m_4$ and $m_2 = m_1(1 + m_3/m_5)$. At this point the derivative of m_5 with respect to m_2 is well defined and is 0 (i.e. the line $m_5 = m_4$ is tangent to the curve at this point). Note also that at this point the three equilibria are equal, and if we pass through it along any straight line in the decreasing direction of m_5, the dynamical system goes from having three equilibrium points (with E_1 stable and the other two unstable) to a single equilibrium point, E_1, which becomes unstable, thus this point is a subcritical pitchfork bifurcation point.

Theorem 7 *The equilibria E_1, E_2 and E_3 of the dynamical system (4) undergo a subcritical pitchfork bifurcation when $m_5 = m_4$ and $m_2 = m_1(1 + m_3/m_5)$.*

Proof See previous remark.

Remark: Once m_1, m_3 and m_4 are taken to be fixed and positive, $\forall\, 0 < m_5 \leq m_4$ it is clear that $m_2 \geq 0$ along the fold bifurcation: If $m_5 \to 0^+, m_2 \to +\infty$ on both branches. On the other hand, the derivative of m_2 with respect to m_5 on the left branch cancels out only if

- $m_5 = m_4 - m_1$ (which implies $m_2 = 0$) when $m_1 < m_4$,
- $m_1 = \dfrac{(m_3 m_4 + m_5^2)^2}{m_3^2(m_4 - m_5)}$ (which implies $m_2 = \dfrac{(m_3 + m_5)^2}{m_3^2(m_4 - m_5)} > 0$) when $m_1 > m_4$.

The pitchfork bifurcation is also present in the positive parametric region, since it lies within the fold bifurcation.

Theorem 8 *A Hopf bifurcation occurs for E_3 when*

$$m_2 = \frac{(m_3 + m_5)^2(m_1 m_3 - m_4 m_3 - m_5^2)}{m_3(m_3 m_4 + m_5^2)}, \tag{10}$$

under the following conditions:

- $m_1 > \dfrac{(m_3 m_4 + m_5^2)^2}{m_3^2(m_4 - m_5)}$,
- $m_4 > m_5$.

Proof The Jacobian Eq. (9) exhibits purely imaginary eigenvalues when $J_{1,1} = 0$ and $J_{1,2} \cdot J_{2,1} < 0$. Let us begin by defining $\overline{L}_i$ as function of the parameters of the system (4). To accomplish this, we examine the following equation given by $J_{1,1} = 0$:

$$\frac{-m_2}{(1 + m_3/m_5)^2}\overline{L}_i^2 + \overline{L}_i\left(m_1 - m_4 - \frac{m_2}{(1 + m_3/m_5)^2}\right) - m_4 = 0.$$

We multiply the equation above by $(1 + m_3/m_5)$ and then calculate its difference with (6), yielding:

$$\overline{L}_i = \overline{L}_H = \frac{m_3 m_4 + m_5^2}{m_1 m_3 - m_3 m_4 - m_5^2}.$$

Substituting $\overline{L}_H$ into $J_{1,1} = 0$, we obtain the first condition for the Hopf bifurcation:

$$m_2 = \frac{(m_3 + m_5)^2(m_1 m_3 - m_4 m_3 - m_5^2)}{m_3(m_3 m_4 + m_5^2)}.$$

With these two conditions (for $\overline{L}_H$ and m_2), substituting we find that $\overline{L}_H$ corresponds to $\overline{L}_3$. Now we need to ensure that the determinant of the Jacobian matrix is positive:

$$\overline{L}_H\left(\frac{m_1}{(1 + \overline{L}_H)^2} - \frac{m_2}{1 + m_3/m_5}\right) > 0.$$

Substituting the explicit forms of $\overline{L}_H$ and m_2, we get the Hopf bifurcation condition,

$$m_1 > \frac{(m_3 m_4 + m_5^2)^2}{m_3^2(m_4 - m_5)} \quad m_4 > m_5. \tag{11}$$

Table 2 Characteristics of the three equilibria of the system for the different regions located in Fig. 1

	Equilibria			
Region	E_1 **(Tumor-free)**	E_2 **(High-tumor)**	E_3 **(Low-tumor)**	**Tumor dynamics**
R_1	**biological significance attractor node**	biological significance saddle	no biological significance saddle	Tumor-free
R_2	biological significance saddle	biological significance saddle	**biological significance attractor node**	Low-tumor control possible
R_3	biological significance saddle	biological significance saddle	**biological significance attractor focus**	Low-tumor control possible
R_{4A}	biological significance saddle	biological significance saddle	biological significance repeller focus + **stable PO**	Low-tumor oscillations control possible
R_{4B}	biological significance saddle	biological significance saddle	biological significance repeller focus	Tumor growing no control
R_5	biological significance saddle	∄	∄	Tumor growing no control
R_6	biological significance saddle	no biological significance **attractor node**	no biological significance saddle	Tumor growing no control
R_7	biological significance saddle	no biological significance **attractor focus**	no biological significance saddle	Tumor growing no control
R_8	biological significance saddle	biological significance saddle	biological significance repeller node	Tumor growing no control
R_9	biological significance saddle	no biological significance saddle	no biological significance **attractor focus**	Tumor growing no control
R_{10}	biological significance saddle	no biological significance saddle	no biological significance **attractor node**	Tumor growing no control

The shaded yellow and green colors are used for biologically important equilibria, shaded green color for controllable tumor, shaded red color for uncontrollable tumor and dark letters for attracting equilibria (Color Figure Online)

Remark: The condition $m_1 > \dfrac{(m_3m_4 + m_5^2)^2}{m_3^2(m_4 - m_5)}$ implies that $m_1 > m_4$. So, if $m_1 \leq m_4$, there is no Hopf bifurcation. In addition, the intersection between the fold bifurcation and the Hopf bifurcation occurs when $m_1 = \dfrac{(m_3m_4 + m_5^2)^2}{m_3^2(m_4 - m_5)}$ that matches the backward (leftmost) point of the fold bifurcation (with $m_2 = \dfrac{(m_3 + m_5)^2}{m_3^2(m_4 - m_5)} > 0$). This codimension-two point (a Bogdanov–Takens bifurcation point) is the origin of the Hopf bifurcation curve.

From the practical point of view, the existence of these bifurcations lead to qualitative changes in the solutions of Eqs. (4), thus having a substantial influence on the populations of lymphoma cells and CAR T-cells.

It is relevant to study the changes of E_i from being of type focus to node, and vice versa. These are not bifurcations since there is no change in the stability, but those changes have implications in the form the solutions converge (or diverge) to (from) equilibria. The analysis is developed in Appendix A.

3.4 Impact of CAR T-Cell Inflow $\sigma(t)$ on the Stability of Equilibria

Figure 1 shows the regions with qualitatively distinct dynamics as functions of the parameters m_2 and m_5 using the explicit formulas obtained in Sec. 3.3. The figure shows also the homoclinic bifurcation curve obtained with the AUTO continuation software (Doedel 1981; Doedel et al. 2000). As discussed in Sec. 3.3, the origin of this bifurcation curve is a Bogdanov–Takens (BT) bifurcation point, also shown in Fig. 1 and determined analytically after Theorem 8.

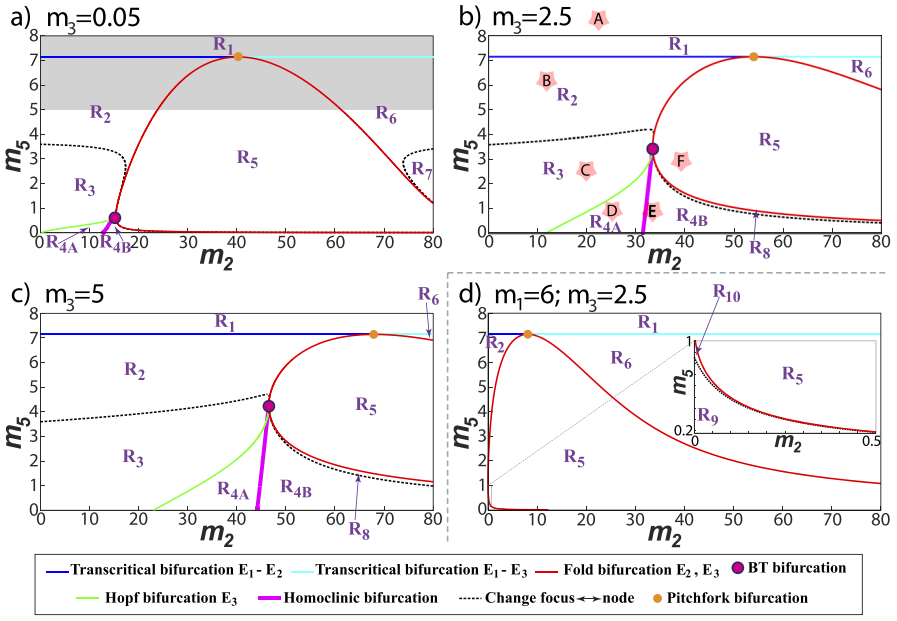

Fig. 1 Different regions of behavior, labeled $R_1 - R_9$, depending on the parameter values m_2, m_5. Three values for m_3 are shown corresponding, for instance to different values of the influx of CAR T-cells into the tumor areas σ: **a** $m_3 = 0.05$, **b** $m_3 = 2.5$ and **c** $m_3 = 5$. The fixed values of the other dimensionless parameters are $m_1 = 40$ and $m_4 = 7.14$. **d** Example with $m_1 = 6, m_3 = 2.5$ corresponding to a case with $m_1 = 6 < m_4$. (see Table 2 for explanation about different regions R_i). The shaded area in subplot **a** lies out of the range of biological interest identified in Table 1. The letters framed by stars in plot **b** indicate the parameter values for the Figs. 2 and 3 (Color Figure Online)

Figure 1a–c shows the regions of stability in the m_2, m_5 plane for three specific choices of m_3. The values chosen for m_3 can be obtained by changing the influxes σ of CAR T-cells into the tumor localization. For instance Fig. 1a corresponds to $\sigma = 10^5$ (lower end of the interval given in Table 1); Fig. 1b to $\sigma = 5 \times 10^6$; and Fig. 1c to $\sigma = 10^7$ (upper end of the interval). In all cases we observe a similar structure of regions but as m_3 (i.e. σ) increases, the regions R_2, R_3 (and R_4) grow, shifting regions R_5-R_8 to the right. This has biological implications since $R_{2,3}$ correspond to the controlled tumor and CAR-T equilibria thus making clear that the maintenance of a flow of CAR T-cells in the system may have a positive effect on maintaining the disease under control. Also, it is clear that achieving a complete cure is only possible in this case for large values of m_5 that can be achieved also by increasing σ. Thus, this appears to be a key parameter able to drive the system in either tumor-free or tumor-controlled scenarios.

Figure 1d shows the case with $m_3 = 2.5$ and $m_1 = 6$ in which there are new regions because $m_1 < m_4$ (see Sec. 3.3). Now the region R_5 is tangent to the axis $m_2 = 0$ and regions $R_{3,4}$ do not exist. Instead the regions R_9 and R_{10} appear. The description of the type of equilibria appearing in each region is listed in Table 2.

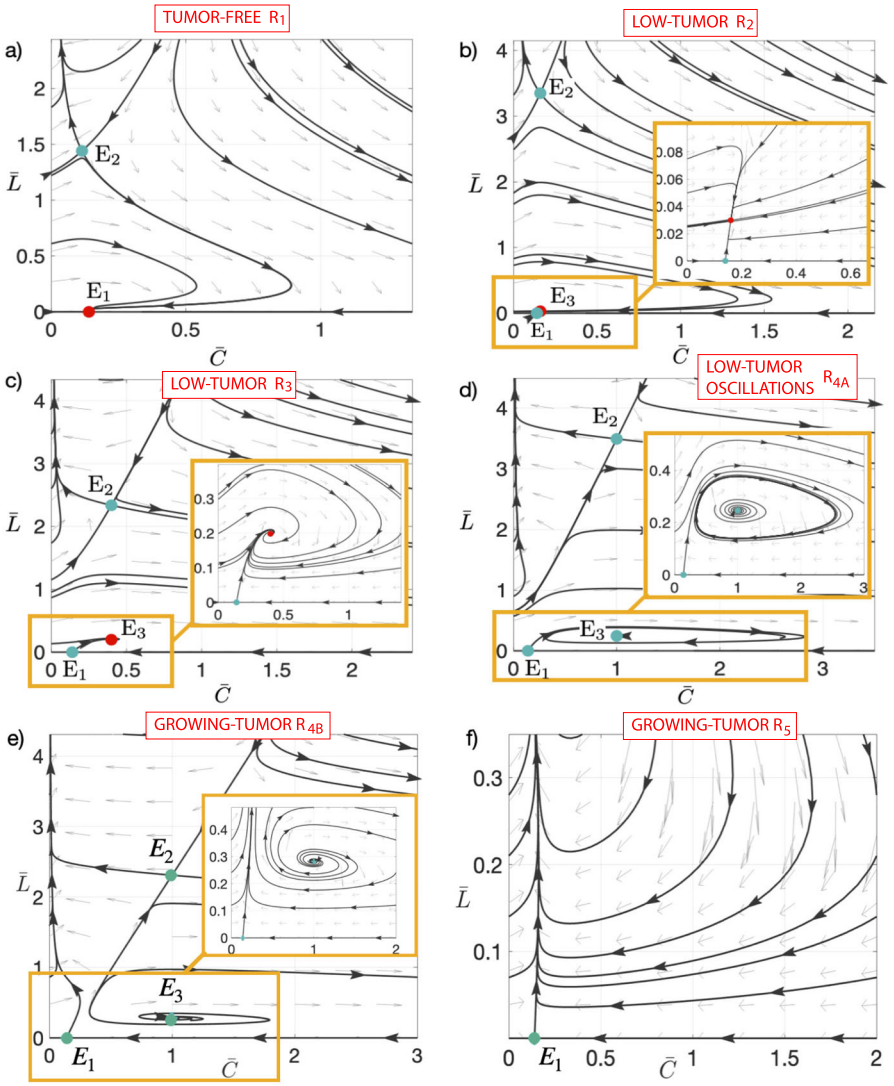

Fig. 2 Phase space portraits for the solutions of Eqs. (4) for different values of the parameters (m_2, m_5). Subplots **a**–**f**, correspond to pairs of values (22, 8.75), in R_1; (12.5, 6.25), in R_2; (20, 2.5), in R_3; (25, 1), in R_{4A}; (33, 1), in R_{4B}; and (40, 3), in R_5 respectively. With these choices, stability of the equilibria fall in the different regions $R_1 - R_5$ discussed in the main text. Other parameters where fixed to $m_1 = 40$, $m_3 = 2.5$ and $m_4 = 7.14$, corresponding with Fig. 1b (Color Figure Online)

3.5 Parameters and Initial Conditions Determine Tumor Control

Representative phase portraits for different pairs of parameters (m_2, m_5) corresponding to the different regions $R_1 - R_5$ are shown in Fig. 2. Note that the dynamics in region R_8 are similar to R_{4B} but the equilibrium E_3 is now an unstable node rather

than an unstable focus. Regions R_6, R_7, R_9 and R_{10} are similar to R_5 because equilibria with different dynamics have no biological meaning, so the interesting dynamics are the same. Therefore, we do not detail the dynamics in these regions. The value of $m_3 = 2.5$ has been fixed as the value of Fig. 1b and other parameters listed in the caption. To study the phase space images in detail we have obtained the stable and unstable manifolds of the saddle equilibria in Fig. 3. Both figures are complementary and each plot of both figures corresponds to the same case (same parameter values and therefore same region). Therefore, we will comment on both figures in parallel.

The three steady states, denoted as E_1, E_2, and E_3, are marked with coloured circles (red for stable equilibrium and green for unstable ones). It can be seen that in Fig. 2a (region R_1) only E_1 and E_2 are positive and just E_1 is stable. The basin of attraction of the equilibrium E_1 occupies a substantial area in the phase space, but there are orbits that are not bounded, corresponding to loss of control of the tumor (see Fig. 3 for the stable and unstable manifolds of the equilibria and the shaded regions in which the tumor escapes the CAR-T surveillance). E_2 is a saddle and its stable manifold ($W^S(E_2)$, shown in green) forms the boundary of the unbounded region (the non-healing region). There is an heteroclinic connection from E_2 to E_1. This orbit also gives a separation in the bounded region, above the heteroclinic cycle the orbits decrease in $\overline{L}$ going to large values of $\overline{C}$ and approaching $\overline{L} = 0$, and converging to E_1. In the remaining area the orbits converge faster to E_1. In practice unbounded orbits are all located in a region with large initial tumor loads and smaller numbers of CAR T-cells infused. This interesting result is fully in line with experimental observations where it is known that factors associated with durable remission after CAR T-cell therapy include lower baseline tumour volume and higher peak circulating CAR T-cell levels (Cappell and Kochenderfer 2023). Similar observations apply in different scenarios when E_1 is unstable but the coexistence equilibrium E_3 is stable as in Figs. 2b,c (see explanation below).

Thus even in a situation where parameters could achieve a cure, the initial situation may have a substantial effect on the outcome, i.e. both parameter values and initial conditions have to be properly engineered to control the system.

It is clear that when the parameter m_5 decreases, which can be associated with the killing efficiency rate α, and m_2 is sufficiently low ($m_2 < m_1(1 + m_3/m_4)$), E_1 becomes unstable, and E_3 appears in the positive quadrant. We have crossed the transcritical bifurcation curve (see Theorem 5). Remarkably, E_3 becomes a stable node, as illustrated in Fig. 2b (region R_2). The situation is quite similar, but a bit more complex, to the one depicted in Fig. 2a. Now the heteroclinic cycles connect E_2 and E_3, and E_1 and E_3. This gives rise to a rather thin path between the stable manifold of E_1 ($W^S(E_1)$) and the heteroclinic cycle between E_2 and E_3. Once an orbit enters its interior, it passes through it towards E_3. The interesting fact is that, although the orbit goes to an endemic equilibrium, the orbit reaches very small values of $\overline{L}$ for a long time before going to E_3. This explains several cases of disease relapse, but also allows us to design strategies to control it before it grows again. In Fig. 2c (region R_3), E_3 is depicted as a stable spiral, reflecting the evolution of its stability characteristics under varying conditions. This stable spiral signifies a more intricate dynamical behavior compared to the stable node observed previously. That is, the only difference is that the orbits oscillate before reaching E_3.

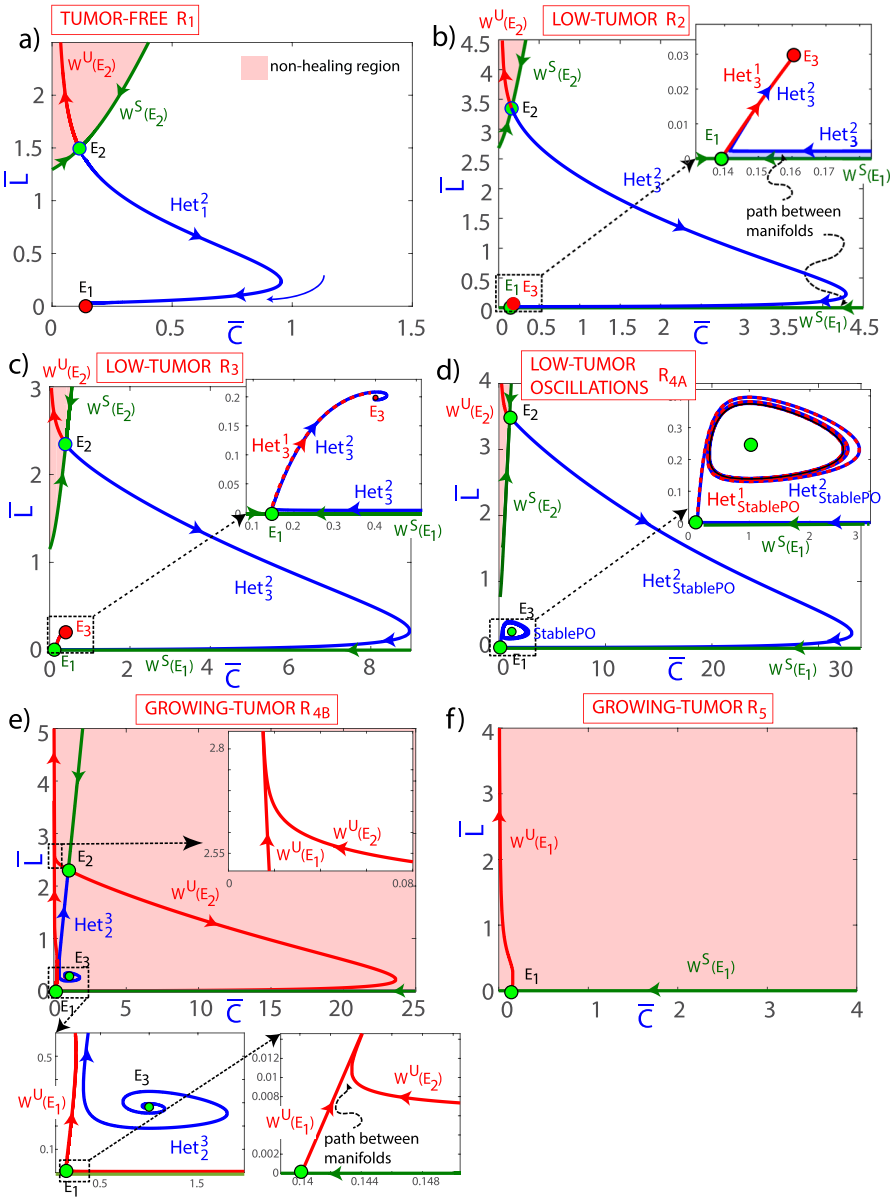

Fig. 3 Stable ($W^s(E_i)$) and unstable ($W^u(E_i)$) manifolds of equilibria on the phase portraits for the solutions of Eqs. (4) for different values of the parameters (m_2, m_5). Subplots **a**–**f**, correspond to pairs of values (22, 8.75) in the R_1 region; (12.5, 6.25) in R_2; (20, 2.5) in R_3; (25, 1) in R_{4A}; (33, 1), in R_{4B}, and (40, 3) in R_5, respectively. Other parameters were fixed to $m_1 = 40, m_3 = 2.5$ and $m_4 = 7.14$. The heteroclinic (Het_i^j) connections among equilibria or the stable periodic orbit are also shown (Color Figure Online)

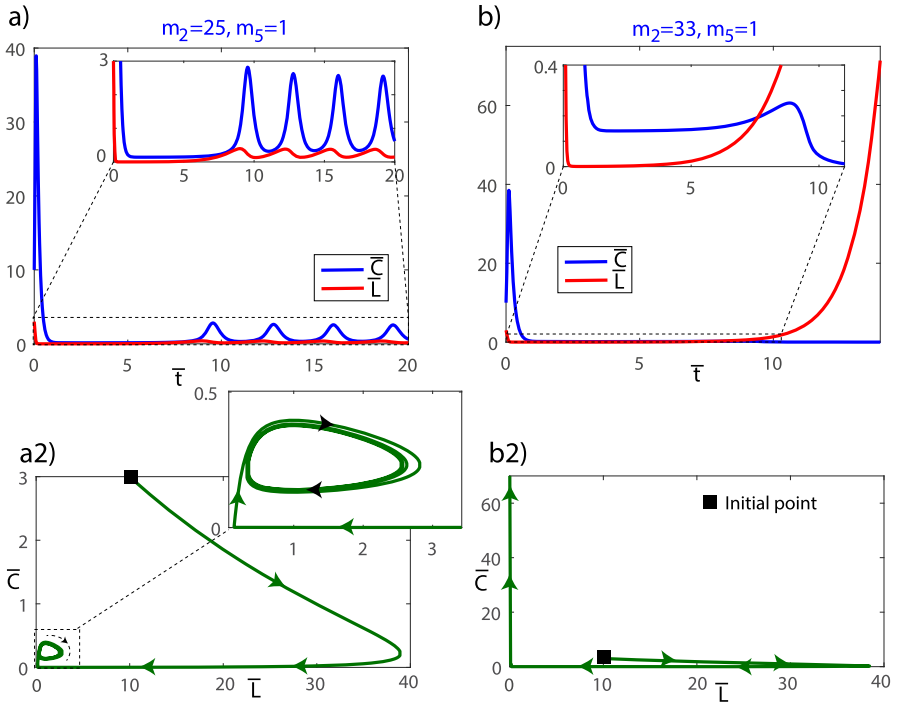

Fig. 4 Examples of the time evolution of orbits in the R_4 region on both sides of the homoclinic bifurcation: **a** $(m_2, m_5) = (25, 1)$ in R_{4A} showing disease control and **b** (33, 1) in R_{4B} displaying tumor escape. Both orbits have the initial conditions $(\bar{C}(0), \bar{L}(0)) = (10, 3)$ in the dimensionless equations (4). **a2** and **b2** show the orbits in the phase space (Color Figure Online)

The behavior of E_3 undergoes a significant change when m_5 decreases and m_2 increases, as depicted in Fig. 2d (region R_{4A}). In this case the E_3 equilibrium point has undergone a supercritical Hopf bifurcation (see Theorem 8). Under such conditions, E_3 transforms into a repeller spiral steady state, and so, the convergence is towards the stable periodic orbit around E_3 generated in the Hopf bifurcation. Note that the heteroclinic cycles lie between equilibria and the stable periodic orbit, but the rest of comments are the same as in plot c). In this region, as m_2 increases and we approach the homoclinic bifurcation curve, the period of the stable limit cycle increases until, upon reaching the homoclinic bifurcation, it becomes a homoclinic orbit of E_1. This is why the limit cycle has disappeared in the R_{4B} region. This bifurcation is quite important and results in a global change to the system. This is the case shown in plot e). Now all the orbits are unbounded, that is, there is no cure or control (if no action is taken). The orbits on the right side can give small values of L but then they enter into two paths between manifolds escaping through them giving rise to unbounded orbits. It is interesting to remark that the escape always follows a nearly vertical line at $C \approx 0$. In Fig. 4 we present the time dynamics of two orbits in the R_4 region: plot a) with $(m_2, m_5) = (25, 1)$ in R_{4A}, and plot b) (33, 1) in R_{4B}. Both orbits have the initial conditions $(\bar{C}(0), \bar{L}(0)) = (10, 3)$ which correspond to a point above the heteroclinic

orbit and to the right of the stable manifold of E_2. In the pictures we can clearly see how after the homoclinic bifurcation (Fig. 4b) the orbit becomes unbounded, whereas in Fig. 4a) the orbit converges to the stable periodic orbit. Note that both orbits stay close to E_1 for some time (quite long, depending on the value of ρ, in case Fig. 2b), meaning that the disease can be controlled for long periods of time with small values of $\bar{L}$. On Fig. 4 a2 and b2 we present these orbits in phase space to gain a better understanding of the dynamics.

Figures 2f and 3f show typical scenarios in R_5 where there is a saddle equilibrium E_1, and all orbits escape. Orbits in regions R_6, R_7, R_9 and R_{10} (not shown) have a similar behavior to those in R_5, since both E_2 and E_3 equilibria exist, but they are not positive. Therefore, the only equilibrium in this quadrant is E_1. Since E_1 is of saddle type in these regions, the dynamics is not bounded and the cancer grows without control. The dynamics in R_8 is similar to that in R_{4B}, with the only difference that the equilibrium E_3 is a (repeller) node instead of a focus, thus all orbits are unbounded.

In summary, within R_1, R_2 and R_3 there is only a stable positive equilibrium point. The value of $\bar{L}$ in those equilibria is either 0 (in R_1) or relatively small (in R_2 and R_3). Thus, it may be possible to cure or take the disease to a stable state controlled by a remnant of CAR T-cells. The equilibrium E_2 is unstable in those regions but determines the dynamics in a part of the phase space. Its stable manifold delimits the bounded region, and above this manifold, the orbits become unbounded, leading to uncontrolled tumor growth. To control the disease, trajectories must reside either within the basin of attraction of E_1 (in R_1) or E_3 (in $R_{2,3}$). It is important to note that equilibrium E_1 is predominantly unstable, except for $m_5 > m_4$, which implies a scenario where CAR T-cells exert significant cytotoxic effects on tumor cells, surpassing the rate of tumor growth and potentially resulting in tumor regression or stabilization over time. When E_1 is unstable, the only control scenario implies converging towards the stable coexistence equilibrium E_3. Regions $R_{2,3}$ increase as σ increases, so a larger inflow of CAR T-cells would make it easier to achieve tumor control. Within regions with controlled tumor growth, the eventual convergence of trajectories towards equilibria (either E_1 or E_3) depends on the specific initial conditions of the system, i.e. the initial number of CAR T-cells and the initial tumor load. In the region R_{4A}, although E_3 is unstable, it is still possible to control the disease due to the existence of an attracting limit cycle generated in the Hopf that delimits this region. This implies that at the time of diagnosis, if the number of lymphoma cells and CAR T-cells are close to the E_3 steady state, it is possible to define a therapeutic protocol capable of taking the patient to a stable disease state. Thus, the model can explain both tumor dormancy and escape from CAR T-cells.

As the value of m_2 increases, indicating an escalation in the tumor inactivating rate γ, in the region R_{4B}, the stable periodic orbit abruptly disappears, consequently leading to an irrevocable non-cure situation. This observation underscores the critical importance and profound impact of the immunosuppressive tumor microenvironment in determining the success or failure of CAR T-cell treatment strategies. It also highlights the intricate interplay between the tumor microenvironment and the efficacy of CAR T-cell therapy, emphasizing the need for a comprehensive understanding of the complex dynamic interactions to enhance treatment outcomes.

4 Study of the Dynamics and Implications for Therapy

In what follows we will work on the dimensional form Eq. (1) of our model in order to facilitate a more insightful analysis and interpretation of our findings.

4.1 Curable Tumor Burden Depends on CAR T-Cell Killing Efficiency and Tumor-Induced Inactivation Rate

To explore the relation between the parameters α and γ and the initial conditions, in Fig. 5 we show different curves obtained by varying the killing efficiency rate α or the tumour inactivity rate γ. The blue curves show the cutoff value of the stable manifold of the equilibrium E_2 with the vertical line $C = 2.5 \times 10^5$. The red curves show the cutoff value of the stable manifold with the straight line $C = 10^8$. Note that the stable manifold of equilibrium E_2 acts as a boundary between the basin of attraction of the stable invariant set and the region of unbounded dynamics, which means the difference between a controlled tumor or an uncontrollable one. Values of L below the blue curve converge to the stable invariant manifold for any value of $C \geq 2.5 \times 10^5$. Values of L above the red curve would require an initial injection of CAR-T above 10^8 cells, that is a large value difficult to reach in realistic scenarios. In other words, the disease would have reached a point at which the therapy would no longer be effective. Between the two curves (coloured area), CAR-T therapy will or will not be effective depending on the initial dose injected. As it can be seen in Fig. 5a), small values of γ would allow the therapy to be effective even with high initial values of L. In contrast, as γ grows (Fig. 5b), larger values of L can quickly prevent the therapy from being effective. The dependence on the α parameter (plot (d)) is essentially linear.

4.2 Short-Term and Long-Term Effects of the Initial Tumor and CAR T-Cell Numbers on the Dynamics

The phase space analysis of Sec. 3.5 has allowed us to study the substantial influence of initial data $C(0)$, $L(0)$ on the disease outcome. We move on now to study the time evolution for different sets of parameters and initial conditions. Let us first consider a tumor inactivation rate $\gamma = 0.4\,\text{day}^{-1}$ and a CAR-T kill rate $\alpha = 2 \times 10^{-10}\,\text{day}^{-1}\,\text{cells}^{-1}$. The remaining parameters were taken to be $\beta = 0.8\,\text{day}^{-1}$, $H = G = 10^8$ cells, $\tau_C = 7$ days, $\sigma = 5 \times 10^6\,\text{cells}\,\text{day}^{-1}$ and $\rho = 0.02\,\text{day}^{-1}$, corresponding to region R_3, $m_2 = 20$ and $m_5 = 2.5$ depicted in Figs. 2c and 3c.

The outcome of the simulations for different initial conditions are summarized in Fig. 6. As expected, the initial number of tumor cells significantly impact treatment outcomes, as illustrated in Fig. 6a. While the disease can be controlled in the short term for small initial tumor cell counts, higher initial tumor loads render CAR T-cells unable to control lymphoma. Interestingly, a non-monotonic trend emerges: with a fixed dose of CAR T-cells, tumor reduction is most effective in the short term at an intermediate initial tumor size. At this level, CAR T-cells receive optimal stimulation from tumor antigens, resulting in robust expansion and efficient tumor clearance. However, at very high tumor burdens, CAR T-cells become overwhelmed, rendering them unable

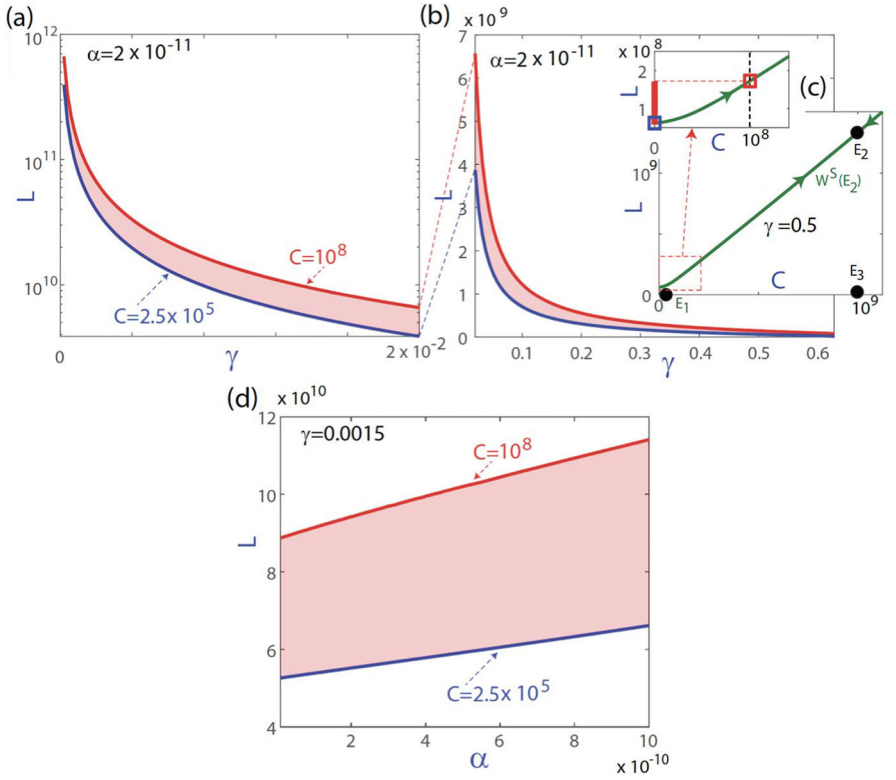

Fig. 5 Ranges of L for which control can be achieved depending on γ and α values. The blue curves show the cutoff value of the stable manifold of the equilibrium E_2 with the vertical line $C = 2.5 \times 10^5$ and the red curves with the vertical line $C = 10^8$. The range of values between both curves show a region in L where the therapy would be effective depending on the initial dose injected. Parameters are $\beta = 0.8\,\text{day}^{-1}$, $H = G = 10^8$ cells, $\tau_C = 7$ days, $\sigma = 5 \times 10^6\,\text{cells}\,\text{day}^{-1}$ and $\rho = 0.02\,\text{day}^{-1}$. **a**, **b** changing γ and fixing $\alpha = 2 \times 10^{-11}\,\text{day}^{-1}$. **c** Graphical explanation of the meaning of the blue and red curves. The shaded area is given by the interval [thick red line in the zoom of subplot (**c**)] among the cutoff value of the stable manifold of the equilibrium E_2 with $C = 2.5 \times 10^5$ and $C = 10^8$. **d** Results varying α and fixing $\gamma = 0.0015\,\text{cells}^{-1} \times \text{day}^{-1}$ (Color figure online)

to control the disease effectively, as the excessive tumor load exceeds their capacity to eliminate the cells. Conversely, while CAR T-cells can still control the disease at very low initial tumor levels, the reduction in tumor cells occurs at a slower rate due to limited antigen stimulation, which restricts the rate of CAR T-cell expansion. This pattern suggests that treatment efficacy does not consistently increase with lower initial tumor loads, highlighting the complexities in CAR T-cell interactions with tumor cells. Therefore, the effectiveness of treatments strongly depends on the initial tumor load.

When the tumor cell number is fixed at 10^8 and the initial values of CAR T-cells are varied within this parameter regime, the dynamics do not significantly change (see Fig. 6b), indicating a weaker dependence of the outcome on the initial CAR T-cell count. However, increasing the initial tumor cell counts ultimately leads to reduced treatment efficacy and potential treatment failure. This behavior is due to the location

of the different initial conditions in different basis of attractions (Figs. 2c and 3c). Using (2) we obtain that $\bar{L}_0 = 10^{-8} L_0$ and $\bar{C}_0 = 4 \times 10^{-9} C_0$, thus when $L_0 = 10^8$ the initial conditions are in the basin of attraction of E_3 regardless of the value of C_0. For higher values of L_0, the value of C_0 would have to be much larger (e.g. of the order of 5×10^8 for $L_0 = 10^9$) to be in such a basin. The influence of the initial number of CAR T-cells is small due to the technical limitation of injecting a large amount of CAR T-cells. There are other situations where initial conditions are not determinant. Taking $\gamma = 0.00015\,\text{day}^{-1}$ and $\alpha = 2 \times 10^{-11}\,\text{day}^{-1}\,\text{cells}^{-1}$, we describe a scenario with a low tumor inactivating rate and a moderate killing efficacy of CAR T-cells against tumor cells. That keeps us in region R_3 (Fig. 1), but now with $m_2 = 7.5 \times 10^{-3}$ and $m_5 = 0.25$. The small value of m_2, due to the low value of γ, makes the equilibrium value of L in E_2 very high (close to 5×10^{12} cells). Thus, in order to enter the escape region, the initial value of L_0 would be around 6×10^{11} cells or higher. This fact can also be seen in Fig. 5, since values of γ close to 0 cause the blue curve to grow rapidly.

Figure 7 illustrates the results obtained for different initial values of lymphoma cells and CAR T-cells for short (panels a,b) and long (panels c,d) times. The results indicate that while the initial conditions have minimal impact on the ultimate treatment outcome, they play a crucial role in determining the timing of the response and the extent of the fold-change reduction in tumor burden. The dynamics converge to an equilibrium E_3 with a small tumour number ($L_3 \approx 2 \times 10^7$ cells). Varying the number of infused CAR T-cells leads to a delay in their expansion (Fig. 7b). Also the peak CAR T-cell expansion depends weakly on the initial number of lymphoma cells (Fig. 7a). Notably, in the short term (Fig. 7a), and as similarly observed in Fig. 6, larger tumors undergo a more pronounced reduction in cell numbers compared to smaller tumors. This phenomenon occurs because larger tumors provide a higher antigen load, which drives robust CAR T-cell activation and proliferation, resulting in a greater absolute reduction in tumor burden. However, in the long term (Fig. 7c), smaller tumors are more effectively controlled and stabilize more rapidly under CAR T-cell pressure, whereas larger tumors require significantly longer to achieve control. These observations highlight that, while CAR T-cell therapy can induce notable short-term tumor reduction, it may be insufficient to sustain long-term disease control, especially in cases of larger tumor burdens.

These simulations show that even in situations where the initial conditions do not significantly affect the overall treatment outcome, they can lead to variations in the timing of certain events, such as the expansion of CAR T-cells and the occurrence of long-term relapses. These observations align with similar findings from previous studies on acute lymphoblastic leukemia (León-Triana et al. 2021b; Martínez-Rubio et al. 2021). Specifically, in scenarios characterized by a low tumor inactivating rate, the initial conditions demonstrate minimal influence on the model's dynamics. However, in contexts with higher tumor inactivating rates, the initial values of tumor cells emerge as critical determinants of treatment success or failure. Interestingly, the initial dose of CAR T-cells only has the capacity to affect the result in a small window of values. Despite the simplicity of our model, it yields pivotal insights that shed light on potential reasons for treatment failures among lymphoma patients and may aid in the identification of treatment responders.

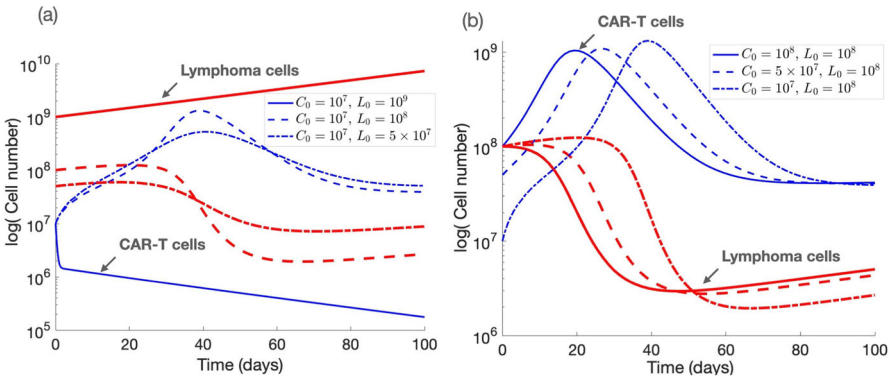

Fig. 6 Dynamics of lymphoma $L(t)$ (red) and CAR-T $C(t)$ (blue) cells. The parameters used fall within the ranges indicated in Table 2.2, with values: $\beta = 0.8\,\text{day}^{-1}$, $H = G = 10^8$ cells, $\tau_C = 7$ days, $\sigma = 5 \times 10^6\,\text{cells}\,\text{day}^{-1}$, $\gamma = 0.4\,\text{day}^{-1}$, $\rho = 0.02\,\text{day}^{-1}$, and $\alpha = 2 \times 10^{-10}\,\text{day}^{-1}\,\text{cells}^{-1}$. **a** Solutions with $L_0 = 5 \times 10^7, 10^8, 10^9$ and $C_0 = 10^7$ over the first 100 days post-treatment. **b** Solutions with $C_0 = 10^7, 5 \times 10^7, 10^8$ and $L_0 = 10^8$ over the first 100 days post-treatment (Color Figure Online)

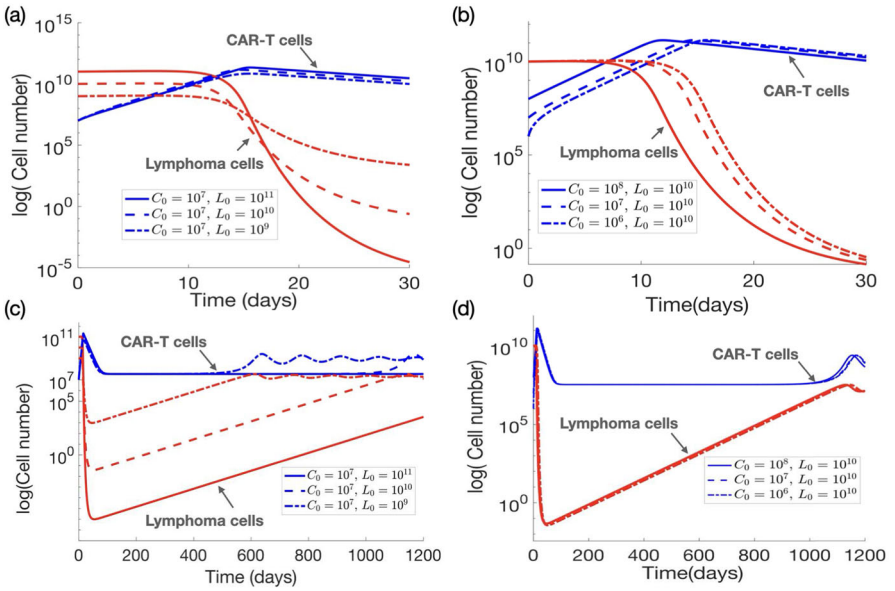

Fig. 7 Dynamics of lymphoma cells $L(t)$ (red lines) and CAR T-cells $C(t)$ (blue) ruled by Eqs. (1) for different initial conditions. Parameters values are $\beta = 0.8\,\text{day}^{-1}$, $H = G = 10^8$ cells, $\tau_C = 7$ days, $\sigma = 5 \times 10^6\,\text{cells}\,\text{day}^{-1}$, $\gamma = 0.00015\,\text{day}^{-1}$, $\rho = 0.02\,\text{day}^{-1}$, and $\alpha = 0.2 \times 10^{-10}\,\text{day}^{-1}\,\text{cells}^{-1}$. (**a**) Dynamics during the first month after treatment, with $C_0 = 10^7$ cells and different values of $L_0 = 10^9, 10^{10}, 10^{11}$ cells. (**b**) Dynamics for $L_0 = 10^{10}$ cells and $C_0 = 10^6, 10^7, 10^8$ cells. **c** and **d** Display long-term evolutions (Color Figure Online)

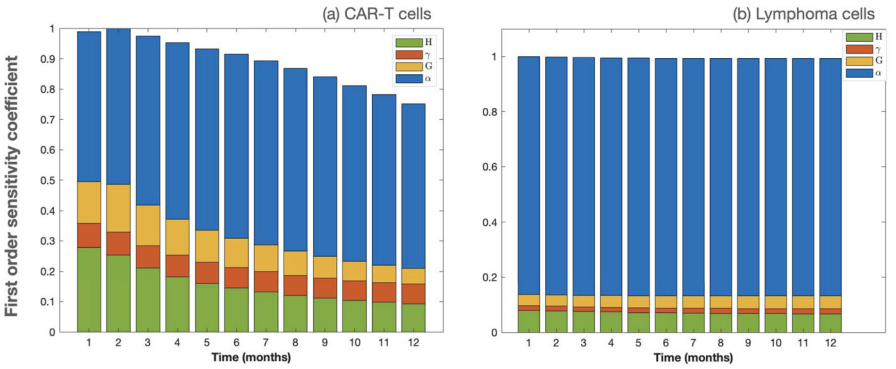

Fig. 8 Sensitivity analysis of Eqs. (1). Parameter values held constant in this analysis were the tumor cell growth rate $\rho = 0.02\,\text{day}^{-1}$, the stimulation rate of CAR T-cells by tumor cells $\beta = 0.8\,\text{day}^{-1}$, the average lifespan of CAR T-cells $\tau_C = 7$ days, and the influx $\sigma = 2 \times 10^5\,\text{cells}\,\text{day}^{-1}$ (Color Figure Online)

4.3 Sensitivity Analysis

We conducted a sensitivity analysis using Sobol's method (Saltelli et al. 2010) to assess the impact of model parameters on the state variables of Eqs. (1). In Fig. 8, we present the first-order sensitivity coefficients to identify the parameters that exert the most significant influence on the dynamics of CAR T-cells and lymphoma cells.

To perform this analysis, we simultaneously perturbed the parameters α, G, γ, and H, as their precise values are not well known. These parameters were subjected to variations within the ranges specified in Table 2.2, while setting the better known parameters to typical values $\rho = 0.02\,\text{day}^{-1}$, $\beta = 0.8\,\text{day}^{-1}$, $\tau_C = 7$ days, $\sigma = 2 \times 10^5\,\text{cells}\,\text{day}^{-1}$.

Notably, the parameter representing the killing efficiency of CAR T-cells against lymphoma emerged as the most influential parameter for both CAR T-cells and lymphoma cells during the first year after injection. This underscores the critical role of CAR T-cell killing efficiency in shaping the dynamics of this therapeutic model.

Parameters H, G, and γ also exert some influence on the dynamics of CAR T-cells. This observation provides further context for our selection of parameter m_2 in the bifurcation analysis discussed in Sec. 3.3.

It is important to note that in our bifurcation analysis, we intentionally focused on varying the values of the parameter γ while keeping H and G constant. This choice reflects the assumption that we can potentially intervene in the inactivation rate γ by administering treatments aimed at reducing the immunosuppression induced by tumor cells, such as PD-1/PD-L1 immune checkpoint inhibitors. This emphasizes the critical role of product attributes in influencing treatment responses and underscores the importance of understanding how these attributes can be modulated to improve therapeutic outcomes.

5 Discussion and Conclusion

CAR T-cell immunotherapy has emerged as a promising treatment for haematological malignancies, yielding encouraging results with high rates of complete remission. In the context of lymphoma, CAR T-cell therapies have also made significant strides in the treatment of relapsed B-cell lymphoma, offering promising rates of sustained remission even in refractory cases although with lower response rates in comparison to leaukemias. Few mathematical models have been developed to specifically characterize the interactions between CAR T-cells and B-cell lymphoma to better understand the different outcomes from treatments.

Our model accounted for the key elements of CAR-T treatments in lymphomas. The two major ones are the expansion of CAR T-cells because of their interaction with cancerous B-cells, either due to direct contacts or through the release of cytokines, and their inactivation due to the immunosupressive effect of cancerous masses. This phenomenon attenuates the therapeutic effect of the drug, and in some cases, hinders disease control. The inclusion of tumor-induced immunosuppression provides insights into treatment failures in certain patients and sheds light on the limitations of CAR T-cell therapy in lymphomas. These cancers share features with solid tumors, and thus often present physical barriers that hinder CAR T-cells from closely interacting with tumor cells.

The primary objective of this research was to conduct a qualitative analysis of the model, aiming to gain a deeper understanding of the dynamics and interactions among lymphoma and CAR T-cells and identifying the key elements influencing their evolution, thus providing hints for therapeutical interventions. Three equilibrium points were found: one representing a tumor-free steady state, and the other two corresponding to coexistence equilibria. We investigated the conditions for these equilibria to be biologically meaningful and examined their stability, which was contingent upon the values of various model parameters.

To comprehensively assess the behavior of cell populations, we performed a bifurcation analysis, with a particular focus on identifying the most influential parameters that shaped population dynamics. Our analysis revealed the existence of distinct types of local bifurcations: transcritical, fold, pitchfork and Hopf bifurcations. Besides, a global homoclinic bifurcation has been found giving a relevant change of behaviour in the system as in one side of this bifurcation all orbits are unbounded. The occurrence of these bifurcations was highly dependent on the values of the key parameters, including α and γ. These parameters respectively characterized the killing capacity of CAR T-cells and the rate of tumor-induced inactivation. The sensitivity analysis also showed that the parameter representing the killing efficiency of CAR T-cells against lymphoma was the most influential one for both CAR T-cells and lymphoma cells during the first year after injection. Thus, the analysis showed that a CAR T-cell product with a high killing capacity can play a pivotal role in disease control and the elimination of lymphoma cells. The effectiveness of the treatment can be assessed based on the quality of the patient's effector cells before genetic modification or the CAR T-cell generation utilized in the therapy. This is in full agreement with the well known critical role of CAR T-cell killing efficiency in shaping the dynamics of this therapeutic concept. Indeed many efforts have been devoted by the biomedical community to develop

'better' CAR products, i.e. those having a faster expansion/killing efficiency (Sterner and Sterner 2021). Furthermore, our model effectively highlighted the relevance of tumor-induced immunosuppression caused by lymphoma cells and its influence on the dynamics of the studied cell populations. Consequently, the utilization of immune checkpoint inhibitors may offer a potential strategy to regulate immune responses, preventing tumor cells from deactivating CAR T-cells. This approach can effectively reduce and control the tumor-induced inactivation rate of CAR T-cells, enhancing the therapeutic outcomes.

We also incorporated a source of CAR T-cells originating from the bloodstream and migrating into the lymph node area. Following injection, CAR T-cells circulate through the bloodstream and migrate into lymphoid tissues, including lymph nodes, where lymphoma cells often accumulate. This migration process is orchestrated by various molecular signals, including chemokines and adhesion molecules, which guide CAR T-cells to the sites of disease manifestation. This external stimulation allowed to extend the basins of attraction of the tumor-controlled equilibria and thus suggests that external supplementation of CAR T-cells could have a role in ensuring the long-term efficacy of the therapy. Currently, the drug is typically administered in the clinics to the patient in a single infusion session using intravenous bags. However, due to the limited impact of the number of injected CAR T-cells in many parameter regimes, using only a portion of the product initially could represent a therapeutic option with similar effectiveness. The remaining product could be preserved for periodic delivery post-response, thereby providing a boost to the internally generated flow of CAR T-cells (σ) and increasing the likelihood of long-term tumor control. Various infusion strategies for CAR T-cell therapy have been explored in the context of clinical trials, including single infusions and fractionated dosing schedules (Frey et al. 2020; Sauter et al. 2019). For example, Frey et al. investigated different CAR T-cell treatment strategies in relapsed/refractory acute lymphoblastic leukemia (r/r ALL), employing fractionated dosing where the total dose is administered incrementally over several days-typically 10% on day 1, 30% on day 2, and 60% on day 3. This method allows for dose adjustments based on patient response, particularly to manage cytokine release syndrome. Studies indicate that fractionated dosing may improve patient safety without compromising efficacy, particularly in adults with r/r ALL, although this is a topic that deserves further clinical investigation.

One of the main results of our analysis was the finding of the key role of the initial tumor load on the outcome, even in parameter regimes with stable tumor-free or tumor-controlled equilibria. This observation aligns with clinical trial results indicating that baseline tumor volume is associated with durable remission following CAR T-cell therapy (Cappell and Kochenderfer 2023). This distinguishes our current model from previously developed mathematical models of CAR T-cell therapy responses in leukemias, which do not account for initial tumor load, in accordance with observations in those cases (León-Triana et al. 2021b). The relevance of the initial tumor load provides an additional justification for the potential effectiveness of bridge therapies currently used after apheresis and before CAR T infusion.

Our modeling approach has some limitations. Notably, we did not incorporate mechanisms directly associated with CAR T-cell exhaustion, which has been observed in various studies as a result of persistent antigen stimulation and an immunosuppres-

sive tumor microenvironment (Gumber and Wang 2022; Kouro et al. 2022). CAR T-cell exhaustion is a gradual loss of function driven by continuous exposure to tumor antigens, leading to diminished efficacy over time. This decline is further accelerated within the tumor microenvironment by the presence of immunosuppressive factors such as regulatory T-cells, myeloid-derived suppressor cells, and inhibitory cytokines. In our model, we captured the inactivation/exhaustion of CAR T-cells by tumor-induced factors as a general representation of immunosuppressive effects. However, this approach does not fully account for the complexity of CAR T-cell exhaustion, including additional contributors such as ligand-independent tonic signaling from CAR structures and the effects of extended in vitro expansion. Incorporating a detailed model of T-cell exhaustion would require a more complex mathematical approach to accurately represent the long-term dynamics of CAR T-cell decline in response to these factors. Such an addition could potentially reveal scenarios of reduced tumor control over prolonged periods, as the model would then capture the gradual functional decay of CAR T-cells as part of the equilibrium state.

The biological factors governing the dynamics of CAR T-cells in our mathematical model include expansion and antigen stimulation, natural cell death, and inactivation by tumor cells. The model should also integrate insights from CAR-T-cell therapy studies, emphasizing the crucial role of achieving sufficient lymphodepletion for a durable and effective treatment response. Consequently, patients undergo lymphodepleting chemotherapy either before or during CAR T-cell infusion, often resulting in a lack of normal B-cells. In line with Kimmel et al. (2021), we deliberately excluded the normal B-cell population from our model for simplicity, as their influence on the dynamics of CAR T-cells and lymphoma B-cells in the lymph node microenvironment is deemed negligible in the short and medium term due to the limited size of that population in patients. This exclusion reduces model complexity and limits the number of parameters needing estimation, making the model more tractable while focusing on the most influential factors.

Furthermore, lymph nodes are distributed in chains or groups throughout various regions of the body, including the throat, armpits, chest, and abdomen. In this article, we have established a simplified mathematical model that describes the dynamics of lymphoma cells and CAR T-cells within a single lymph node group. To gain a more comprehensive understanding of this dynamic, it would be beneficial to extend our mathematical model to study the interactions between these cell populations throughout the entire body. This expansion would involve multiple compartments and would offer a more detailed depiction of the interactions between lymphoma cells and CAR T-cells across different lymph nodes and the circulation of CAR T-cells between the bloodstream and the lymphatic system.

Lastly, it is important to acknowledge the significance of spatial effects in the context of CAR T-cell therapy, particularly in the case of diffuse large B-cell lymphoma. While our model has provided valuable insights into the dynamics of CAR T-cell interactions with lymphoma cells, spatial considerations play a key role in shaping those interactions. Current mathematical models of CAR-T treatments of haematological malignancies have not explicitly addressed spatial effects, relying instead on the assumption that all CAR T-cells are in contact with all tumor cells. Thus, future

works in CAR T-cell modeling should incorporate the impact of spatial constraints on treatment efficacy.

Overall, our study contributes to the relatively sparse body of mathematical research focused on lymphoma response to CAR T-cell therapy. We hope that our findings could serve as a catalyst for further mathematical investigations in this area, ultimately helping to optimize and personalize cellular immunotherapy treatment strategies for lymphoma patients.

Appendix A: Changes in Equilibria Types That Do Not Imply changes in Stability

It is also interesting to study the changes of E_i from being of type focus to type node, or vice versa. Although these are no bifurcations since there is no change in the stability of the equilibria, those changes have implications for how the solutions converge (or diverge) to (from) equilibria. First, if

$$m_1 \geq \frac{-4m_3^2m_4 + m_3^2m_4^2 + (4m_3^2 - 8m_3m_4)m_5 + (8m_3 - 4m_4 + 2m_3m_4)m_5^2 + 4m_5^3 + m_5^4}{m_3^2(m_4 - m_5)} \tag{A1}$$

and E_i with $i = 2, 3$ is an attractor (or repeller), then there is a change in the type of attractor (from focus to node or vice versa) when

$$m_2 = \frac{(m_3 + m_5)^2\left[k_1 - m_1(k_2 + k_3 + k_4) + 2(k_5 + k_6 + k_7 + k_8 + 2m_4m_5^5 - 2m_5^6 \pm \sqrt{k_9})\right]}{m_5p_1\left[p_2 + 2m_3m_5(m_4(-4 + m_5) + 4m_5) + m_5^2(-4m_4 + m_5(4 + m_5))\right]}, \tag{A2}$$

with

$$\begin{aligned}
k_1 &= m_1^2m_3^2(m_3(m_4(-4 + m_5) + 4m_5) + m_5(-4m_4 + m_5(4 + m_5))),\\
k_2 &= m_3^3(-8m_4(-2 + m_5) + m_4^2m_5 + 4(-4 + m_5)m_5),\\
k_3 &= -4m_5^3(-4m_4 + m_5(4 + m_5)) + 2m_3^2m_5(2(-12 + m_5)m_5 + m_4(24 - 8m_5 + m_5^2)),\\
k_4 &= m_3m_5^2(-8m_4(-6 + m_5) + m_5(-48 - 4m_5 + m_5^2)),\\
k_5 &= -8m_3^3m_4^2 + 2m_3^3m_4^3 + 16m_3^3m_4m_5 - 24m_3^2m_4^2m_5 - 2m_3^3m_4^2m_5,\\
k_6 &= 2m_3^2m_4^3m_5 - 8m_3^3m_5^2 + 48m_3^2m_4m_5^2 - 24m_3m_4^2m_5^2,\\
k_7 &= 2m_3^2m_4^2m_5^2 - 24m_3^2m_5^3 + 48m_3m_4m_5^3 - 4m_3^2m_4m_5^3 - 8m_4^2m_5^3,\\
k_8 &= 4m_3m_4^2m_5^3 - 24m_3m_5^4 + 16m_4m_5^4 - 2m_3m_4m_5^4 - 8m_5^5 - 2m_3m_5^5,\\
k_9 &= -m_1(r_1 + r_2)(r_3 + r_4)^2,
\end{aligned}$$

where

$$p_1 = \left[(4 + m_1)m_3^2 + 8m_3m_5 + 4m_5^2\right],$$

$$p_2 = m_3^2(-4m_4 + m_4^2 + 4m_5),$$

and

$$\begin{aligned}
r_1 &= 2m_3m_5(m_4(-4 + m_5) + 4m_5),\\
r_2 &= m_3^2\left[-(4 + m_1)m_4 + m_4^2 + (4 + m_1)m_5) + m_5^2(-4m_4 + m_5(4 + m_5)\right],\\
r_3 &= 2m_3m_5(m_4(-8 + m_5) + 8m_5),\\
r_4 &= m_3^2\left[-(8 + m_1)m_4 + m_4^2 + (8 + m_1)m_5) + m_5^2(-8m_4 + m_5(8 + m_5)\right].
\end{aligned}$$

Acknowledgements This work has been partially supported by project PID2022-142341OB-I00, funded by Ministerio de Ciencia e Innovación/Agencia Estatal de Investigación. Spain (doi:10.13039/501100011033) and European Regional Development Fund (ERDF A way of making Europe); grant SBPLY/21/180501/000145 (Junta de Comunidades de Castilla-La Mancha, Spain) and ERDF; and grant 2022-GRIN-34405 funded by University of Castilla-La Mancha/FEDER (Applied Science Projects within the UCLM research programme). RB and SS have been supported by the Spanish Research project and TED2021-130459B-I00 and by the European Regional Development Fund and Diputación General de Aragón (E24-23R, E24-20R and LMP94-21). SS has been supported by the Spanish Research project PID2019-105674RB-I00.

Funding Open Access funding provided thanks to the CRUE-CSIC agreement with Springer Nature.

References

Adhikarla V, Awuah D, Brummer AB, Caserta E, Krishnan A, Pichiorri F, Minnix M, Shively JE, Wong JYC, Wang X, Rockne RC (2021) A mathematical modeling approach for targeted radionuclide and chimeric antigen receptor T cell combination therapy. Cancers 13:5171. https://doi.org/10.3390/cancers13205171

Baker DJ, Arany Z, Baur JA, Epstein JA, June CH (2023) CAR T therapy beyond cancer: the evolution of a living drug. Nature 619:707–715. https://doi.org/10.1038/s41586-023-06243-w

Barros LRC, Paixão EA, Valli AMP, Naozuka GT, Fassoni AC, Almeida RC (2021) CARTmath—a mathematical model of CAR-T immunotherapy in preclinical studies of hematological cancers. Cancers 13(12):2941. https://doi.org/10.3390/cancers13122941

Bodnar M, Foryś U, Piotrowska MJ, Bodzioch M, Romero-Rosales JA, Belmonte-Beitia J (2023) On the analysis of a mathematical model of CAR T-cell therapy for glioblastoma: insights from a mathematical model. Int J Appl Math Comput Sci 33(3):379–394. https://doi.org/10.34768/AMCS-2023-0027

Brummer AB, Yang X, Ma E, Gutova M, Brown CE, Rockne RC (2022) Dose-dependent thresholds of dexamethasone destabilize CAR T-cell treatment efficacy. PLoS Comput Biol 18:e1009504. https://doi.org/10.1371/journal.pcbi.1009504

Cappell KM, Kochenderfer JN (2023) Long-term outcomes following CAR T cell therapy: what we know so far. Nat Rev Clin Oncol 20(6):359–371

Cheever A, Townsend M, O'Neill K (2022) Tumor microenvironment immunosuppression: a roadblock to CAR T-cell advancement in solid tumors. Cells 11(22):3626. https://doi.org/10.3390/cells11223626

Davenport AJ, Jenkins MR, Ritchie DS, Prince HM, Trapani JA, Kershaw MH, Darcy PK, Neeson PJ (2015) CAR T-cells are serial killers. OncoImmunology 4(12):e1053684. https://doi.org/10.1080/2162402x.2015.1053684

Doedel E (1981) AUTO: a program for the automatic bifurcation analysis of autonomous systems. In: Proceedings of the tenth Manitoba conference on numerical mathematics and computing, vol I (Winnipeg, Man., 1980), vol 30, pp 265–284

Doedel EJ, Paffenroth RC, Champneys AR, Fairgrieve TF, Kuznetsov YA, Oldeman BE, Sandstede B, Wang XJ. Auto2000. http://cmvl.cs.concordia.ca/auto

Frey NV, Shaw PA, Hexner EO et al (2020) Optimizing chimeric antigen receptor T-cell therapy for adults with acute lymphoblastic leukemia. JCO 38(5):415–422. https://doi.org/10.1200/JCO.19.01892

Frølund UC, Nielsen SL, Hansen PB (2011) Burkitt lymphoma is a highly malign tumour with a doubling time of twenty-four hours. Ugeskr Laeger 173(43):2714–2718

Ganesh SR, Roth CM, Parekkadan B (2023) Simulating interclonal interactions in diffuse large B-cell lymphoma. Bioengineering 10(12):1360. https://doi.org/10.3390/bioengineering10121360

Ghorashian S, Kramer AM, Onuoha S et al (2019) Enhanced CAR T cell expansion and prolonged persistence in pediatric patients with ALL treated with a low-affinity CD19 CAR. Nat Med 25:1408–1414. https://doi.org/10.1038/s41591-019-0549-5

Guckenheimer J, Holmes P (1983) Nonlinear oscillations, dynamical systems, and bifurcations of vector fields. Springer, New York. https://doi.org/10.1007/978-1-4612-1140-2

Gumber D, Wang LD (2022) Improving CAR-T immunotherapy: overcoming the challenges of T cell exhaustion. EBioMedicine 77:103941. https://doi.org/10.1016/j.ebiom.2022.103941

Kimmel GJ, Locke FL, Altrock PM (2021) The roles of T cell competition and stochastic extinction events in chimeric antigen receptor T cell therapy. Proc R Soc B. https://doi.org/10.1098/rspb.2021.0229

Kouro T, Himuro H, Sasada T (2022) Exhaustion of CAR T cells: potential causes and solutions. J Transl Med. https://doi.org/10.1186/s12967-022-03442-3

Kuznetsov V, Makalkin I, Taylor M, Perelson A (1994) Nonlinear dynamics of immunogenic tumors: parameter estimation and global bifurcation analysis. Bull Math Biol 56(2):295–321. https://doi.org/10.1016/s0092-8240(05)80260-5

Lang W, Kienzle S, Diehl V (1980) Proliferation kinetics of malignant non-Hodgkin's lymphomas related to histopathology of lymph node biopsies. Virchows Arch A Path Anat Histol 389(3):397–407. https://doi.org/10.1007/bf00430662

León-Triana O, Pérez-Martínez A, Ramírez-Orellana M, Pérez-García VM (2021a) Dual-target CAR-Ts with on- and off-tumour activity may override immune suppression in solid cancers: a mathematical proof of concept. Cancers 13(4):703. https://doi.org/10.3390/cancers13040703

León-Triana O, Sabir S, Calvo GF, Belmonte-Beitia J, Chulián S, Martínez-Rubio Á, Rosa M, Pérez-Martínez A, Ramirez-Orellana M, Pérez-García VM (2021b) CAR T cell therapy in B-cell acute lymphoblastic leukaemia: insights from mathematical models. Commun Nonlinear Sci Numer Simul 94:105570. https://doi.org/10.1016/j.cnsns.2020.105570

Li R, Sahoo P, Wang D, Wang Q, Brown CE, Rockne RC et al (2023) Modeling interaction of Glioma cells and CAR T-cells considering multiple CAR T-cells bindings. ImmunoInformatics 9:100022. https://doi.org/10.1016/j.immuno.2023.100022

Liu L, Ma C, Zhang Z, Witkowski MT, Aifantis I, Ghassemi S, Chen W (2022) Computational model of CAR T-cell immunotherapy dissects and predicts leukemia patient responses at remission, resistance, and relapse. J Immunother Cancer 10(12):e005360. https://doi.org/10.1136/jitc-2022-005360

Mahasa KJ, Ouifki R, Eladdadi A, de Pillis L (2022) A combination therapy of oncolytic viruses and chimeric antigen receptor T cells: a mathematical model proof-of-concept. Math Biosic Eng 19(5):4429–57. https://doi.org/10.3934/mbe.2022205

Martínez-Rubio Á, Chulián S, Blázquez Goñi C, Ramírez Orellana M, Pérez Martínez A, Navarro-Zapata A, Ferreras C, Pérez-García VM, Rosa M (2021) A mathematical description of the bone marrow dynamics during CAR T-cell therapy in B-cell childhood acute lymphoblastic leukemia. Int J Mol Sci 22(12):6371. https://doi.org/10.3390/ijms22126371

Nayar S, Dasgupta P, Galustian C (2015) Extending the lifespan and efficacies of immune cells used in adoptive transfer for cancer immunotherapies—a review. OncoImmunology 4(4):e1002720. https://doi.org/10.1080/2162402x.2014.1002720

Ocaña-Tienda B, Pérez-Beteta J, Jiménez-Sánchez J, Molina-García D, Ortiz de Mendivil A, Asenjo B, Albillo D, Pérez-Romasanta LA, Valiente M, Zhu L, García-Gómez P, González-Del Portillo E, Llorente M, Carballo N, Arana E, Pérez-García VM (2023) Growth exponents reflect evolutionary

processes and treatment response in brain metastases. npj Syst Biol Appl 9(1):35. https://doi.org/10.1038/s41540-023-00298-1
Owens K, Bozic I (2021) Modeling CAR T-cell therapy with patient preconditioning. Bull Math Biol 83(5):42. https://doi.org/10.1007/s11538-021-00869-5
Pérez-García VM, Calvo GF, Bosque JJ, León-Triana O, Jiménez J, Pérez-Beteta J, Belmonte-Beitia J, Valiente M, Zhu L, García-Gómez P, Sánchez-Gómez P, Hernández-San Miguel E, Hortigüela R, Azimzade Y, Molina-García D, Martínez Á, Acosta Rojas Á, Ortiz de Mendivil A, Vallette F, Schucht P, Murek M, Pérez-Cano M, Albillo D, Honguero Martínez AF, Jiménez Londoño GA, Arana E, García Vicente AM (2020) Universal scaling laws rule explosive growth in human cancers. Nat Phys 16(12):1232–7. https://doi.org/10.1038/s41567-020-0978-6
Pérez-García VM, León-Triana O, Rosa M, Pérez-Martínez A (2021) CAR T cells for T-cell leukemias: insights from mathematical models. Commun Nonlinear Sci Numer Simul 96:105684. https://doi.org/10.1016/j.cnsns.2020.105684
Roesch K, Hasenclever D, Scholz M (2013) Modelling lymphoma therapy and outcome. Bull Math Biol 76(2):401–30. https://doi.org/10.1007/s11538-013-9925-3
Sahoo P, Yang X, Abler D, Maestrini D, Adhikarla V, Frankhouser D, Cho H, Machuca V, Wang D, Barish M, Gutova M, Branciamore S, Brown CE, Rockne RC (2020) Mathematical deconvolution of CAR T-cell proliferation and exhaustion from real-time killing assay data. J R Soc Interface 17(162):20190734. https://doi.org/10.1098/rsif.2019.0734
Saltelli A, Annoni P, Azzini I, Campolongo F, Ratto M, Tarantola S (2010) Variance based sensitivity analysis of model output. Design and estimator for the total sensitivity index. Comput Phys Commun 181(2):259–70. https://doi.org/10.1016/j.cpc.2009.09.018
Santurio DS, Paixão EA, Barros LRC, Almeida RC, Fassoni AC (2024) Mechanisms of resistance to CAR T-cell immunotherapy: insights from a mathematical model. Appl Math Model 125:1–15. https://doi.org/10.1016/j.apm.2023.08.029
Sauter CS, Senechal B, Rivière I et al (2019) CD19 CAR T cells following autologous transplantation in poor-risk relapsed and refractory B-cell non-Hodgkin lymphoma. Blood 134(7):626–635. https://doi.org/10.1182/blood.2018883421
Sehn LH, Salles G (2021) diffuse large B-cell lymphoma. N Engl J Med 384(9):842–58. https://doi.org/10.1056/nejmra2027612
Serrano S, Barrio R, Martínez-Rubio A, Belmonte-Beitia J, Pérez-García VM (2024) Understanding the role of B-cells in CAR T-cell therapy in leukemia through a mathematical model. Chaos Interdiscip J Nonlinear Sci 34(8):083142. https://doi.org/10.1063/5.0206341
Sheikh S, Migliorini D, Lang N (2022) CAR T-based therapies in lymphoma: a review of current practice and perspectives. Biomedicines 10(8):1960. https://doi.org/10.3390/biomedicines10081960
Stein AM, Grupp SA, Levine JE, Laetsch TW, Pulsipher MA, Boyer MW, August KJ, Levine BL, Tomassian L, Shah S, Leung M, Huang P, Awasthi R, Mueller KT, Wood PA, June CH (2019) Tisagenlecleucel model-based cellular kinetic analysis of chimeric antigen receptor-T cells. CPT Pharmacom Syst Pharma 8(5):285–95. https://doi.org/10.1002/psp4.12388
Sterner RC, Sterner RM (2021) CAR T-cell therapy: current limitations and potential strategies. Blood Cancer J 11:69. https://doi.org/10.1038/s41408-021-00459-7
Thandra KC, Barsouk A, Saginala K, Padala SA, Barsouk A, Rawla P (2021) Epidemiology of non-Hodgkin's lymphoma. Med Sci 9(1):5. https://doi.org/10.3390/medsci9010005
Tubiana M (1989) Tumor cell proliferation kinetics and tumor growth rate. Acta Oncol 28(1):113–21. https://doi.org/10.3109/02841868909111193
Viola A, Lanzavecchia A (1996) T cell activation determined by T cell receptor number and tunable thresholds. Science 273:104–106. https://doi.org/10.1126/science.273.5271.104
Wang SS (2023) Epidemiology and etiology of diffuse large B-cell lymphoma. Semin Hematol 60(5):255–266. https://doi.org/10.1053/j.seminhematol.2023.11.004
Weigelin B, Friedl P (2022) T cell-mediated additive cytotoxicity death by multiple bullets. Trends Cancer 8(12):980–987. https://doi.org/10.1016/j.trecan.2022.07.007
Weigelin B, den Boer AT, Wagena E, Broen K, Dolstra H, de Boer RJ, Figdor CG, Textor J, Friedl P (2021) Cytotoxic T cells are able to efficiently eliminate cancer cells by additive cytotoxicity. Nat Commun 12(1):5217. https://doi.org/10.1038/s41467-021-25282-3
Wiggins S (2003) Introduction to applied nonlinear dynamical systems and chaos. Springer, Berlin. https://doi.org/10.1007/b97481

Zhang X, Zhu L, Zhang H, Chen S, Xiao Y (2022) CAR T-cell therapy in hematological malignancies: current opportunities and challenges. Front Immunol 13:927153. https://doi.org/10.3389/fimmu.2022.927153